R. & M. No. 3471

R. & M. No. 3471

MINISTRY OF AVIATION

AERONAUTICAL RESEARCH COUNCIL

The Calculation of the Warp to Produce a Given Load and the Pressures due to a Given Thickness on Thin Slender Wings in Supersonic Flow

By J. H. B. Smith, J. A. Beasley,
Diana Short and F. Walkden

LONDON: HER MAJESTY'S STATIONERY OFFICE

1967

PRICE 13*s.* 6*d.* NET

The Calculation of the Warp to Produce a Given Load and the Pressures due to a Given Thickness on Thin Slender Wings in Supersonic Flow

By J. H. B. Smith, J. A. Beasley,
Diana Short and F. Walkden

Reports and Memoranda No. 3471*
November, 1965

Summary.

According to the linearized theory of supersonic flow, both the local slope of the mean surface of a wing producing a specified distribution of lift and the pressure on a wing due to a specified distribution of volume are given as singular double integrals. The numerical evaluation of these is described for planforms with curved subsonic leading edges and supersonic trailing edges for the cases in which the lift distribution tends to zero like the square root of the distance from the leading edge and the volume distribution has a finite slope there. Examples are given illustrating the use of these methods in the design of slender wings.

LIST OF CONTENTS

*Replaces R.A.E. Tech. Report No. 65260 – A.R.C. 27547.

1. *Introduction.*

1.1. *The Aerodynamic Background.*

In order to make clear why the work here presented was undertaken and how the particular problems treated arise, it is necessary to outline the background of thinking about aerodynamic design into which they fit.

A delta-like, all-wing configuration with curved subsonic* leading edges and supersonic* trailing edges has been proposed[1,2,3] for a transport aircraft to operate economically at a Mach number near 2. On such a configuration, a single type of flow can be maintained throughout the range of conditions encountered in flight, with the reduction in aerodynamic complexity that ensues. Such a flow separates from all edges of the wing, from the trailing edge in the familiar fashion and from each leading edge to form a single vortex lying inboard of the edge.

To produce a flow of this type the edges must be aerodynamically sharp, so that separation is fixed at them, and rapid variations of sweep along the leading edge must be avoided, so that the vorticity shed from the leading edge can all join a single vortex growing more or less uniformly along its length. To avoid the possibility that, at some incidence, vorticity might be shed towards the upper surface of the wing from some part of the leading edge and towards the lower surface from another part, there must be an incidence at which the leading edge is an attachment line. This, sometimes called the ideal incidence, will be called the attachment incidence in this report and the corresponding lift coefficient will be called the attachment lift coefficient. If boundary-layer separation forward of the trailing edge is avoided at the attachment incidence, it is likely that the primary separations from the leading edges will dominate any secondary separations elsewhere on the wing at other incidences. Strictly, only an unwarped wing can have attachment lines along its leading edges through a range of subsonic and supersonic Mach numbers, and only at supersonic speeds can unfavourable pressure fields be avoided. However, suppose this design condition in which the flow is attached along the leading edges and separation is avoided forward of the trailing edge is achieved at the cruise Mach number at an incidence not exceeding the cruising incidence. Then, since the range of incidences required at lower speeds is likely to be above this (and well above it in the critical approach condition), it is reasonable to suppose that the separation from the whole of the leading edge will always be directed towards the same surface of the wing and that it will dominate any other separation which occurs. In order to avoid separation of the three-dimensional boundary layer at the design condition it is known[4,5] that it is sufficient to produce a pressure field on the wing in which the pressure falls both in the mainstream direction and inwards from the leading edge to the centreline; just how steep an adverse gradient in either direction a turbulent boundary layer will withstand can only be determined experimentally at present.

---

*An edge is called subsonic if the component of the free-stream velocity normal to it is everywhere less than the free-stream speed of sound and supersonic if the component everywhere exceeds the sound speed.

The type of flow which has just been described is obtained on unwarped wings of a variety of delta-like planforms and smooth distributions of volume. Moreover, if such a wing has a span of the order of one-half of its length, the lift it produces is usually adequate for conventional landing at currently accepted speeds and feasible attitudes[2]. Unwarped wings, however, are not ideal for aircraft of the type under consideration. The lift-dependant drag of suitably warped wings is lower than that of unwarped wings[6,7,8] both at supersonic and subsonic speeds, even though the lift vector on the unwarped wings is inclined forward of the normal to the wing plane. Linearized theory, too, predicts a reduction in lift-dependent drag from the application of warp to delta wings[9]. In addition, if the centre of gravity of an unwarped delta-like wing is fixed to provide natural longitudinal stability at the approach condition, the lift at a Mach number near 2 will act some 7 to 8 per cent of the length further aft[2], giving rise to a problem of trim[10]. A form of warp which results in a smooth redistribution of lift towards the front of the wing at cruise is the easiest way to solve this problem. The design problem now becomes one of the application of warp to secure trim and low drag without compromising the unified flow and high lift at a given attitude obtainable on the unwarped wing.

Here the properties which have been demanded for the wing at the design point all combine to make the problem tractable. The planform is pointed and the leading edges are sharp and subsonic, so the bow shock is attached and weak. Experiments on wings with unswept trailing edges reveal no significant upstream influence of the trailing-edge shock system, which can therefore be regarded simply as the first stage of the process by which free-stream conditions are regained behind the wing. Viscous effects are confined to these shocks and to the boundary layer, which remains attached forward of the trailing edge at the design point. The disturbance velocities produced by the wing are small, owing to the low wing loading, the vanishing of the local load along the leading edges and the choice of a volume distribution to give a low wave-drag and sharp leading edges. The wing is almost planar and its planform has a smooth leading edge. The cruise Mach number is at once well above the transonic range and well below the hypersonic range, so that no obstacle to the linearization of the governing equations arises. These circumstances combine to make the situation ideal for the application of the linearized theory of supersonic flow past thin wings; moreover, the measure of success achieved by two approximations to it, slender thin-wing theory[6,8] and not-so-slender thin-wing theory[7], gives confidence in its use.

Within this theory, the volume and lifting properties of the wing are separable. The pressure at a point due to a given distribution of volume over the planform can be evaluated directly, and the local streamwise slope of the mean surface can also be found directly from the distribution of lift over the planform; 'directly' in the sense that their evaluation depends on the calculation of integrals, rather than the solution of integral equations. If a volume distribution has been chosen (on grounds of lay-out, structure and wave-drag, say), the pressure distribution it produces can be found. This pressure distribution gives a useful guide as to whether the inviscid flow, on which the calculation of both wave-drag and pressure is based, is a sensible approximation to a real flow. In particular, if the pressure field over the wing is favourable to boundary-layer development and the predicted suction at the trailing edge is not too high, the type of flow with an attached boundary layer forward of the trailing edge and no upstream movement of the trailing-edge shock system can be expected to occur. A lift distribution can then be chosen so that the combined pressure field is, as far as possible, favourable; so that the leading edges are attachment lines; and so that an appropriate pitching moment for trim and an appropriate lift are obtained. This lift distribution leads to the wing warp. If the lift chosen were that at which the aircraft was to cruise, the distribution used in the design would be that corresponding to the cruise condition and it would be chosen to keep the lift-dependent drag low, using the expression for the drag in terms of the lift distribution as given by Lomax[11]. Although estimates of lift-dependent drag based on linearized theory are notoriously unreliable, they might well be of more use in this case in which the leading edges are attachment lines.

Measurements[12] made on wings designed by slender thin-wing theory have shown that the large amount of leading-edge droop associated with an attachment lift coefficient as high as the cruise lift coefficient ($C_L \simeq 0{\cdot}1$) has reduced the available lift coefficient at the approach to an unacceptable extent, whereas smaller amounts of droop have had very much less effect[6]. Other measurements[6,7,8] on the same and similar wings have shown that lower values of the lift-dependent drag factor, C_D/C_L^2, are found at lift

coefficients above the attachment lift coefficient, presumably as a result of the action of the suction under the leading-edge vortex on the forward-facing drooped surface. Although the full linearized theory produces less droop than the slender thin-wing theory for the same lift distribution if $M > 1$ (*see* Fig. 6 of Ref. 13, for example), these observations make it likely that the attachment lift coefficient would be chosen below the cruising lift coefficient. Because the flow is separated, there is then no theoretical relation between the drag at cruise and the lift distribution chosen for the design. However, considerations derived from the drag at cruise can still be applied to the choice of lift distribution, as will be seen in the example discussed in Section 5.2 below.

From the foregoing it is clear that, once the volume distribution of the wing has been fixed and the pressure field due to volume found, nearly all the properties required of the wing can readily be specified in terms of the lift distribution over it at its attachment incidence. The linearized theory of supersonic flow past thin wings, which. as indicated, is expected to be sufficiently reliable, provides expressions both for the pressure due to a given volume distribution and for the surface slope required to induce a given lift distribution. The work here reported on was undertaken to obtain from these expressions sufficiently flexible digital computer programmes to enable design processes, along the lines set out above, to be carried through. An account[14] of the major part of the numerical analysis has previously received a limited circulation.

1.2. *The Nature of the Present Contribution.*

The starting point is a review, from the point of view of numerical calculation, of the familiar expressions for the pressure due to a distribution of volume and for the surface slope needed to induce a given distribution of lift. Although these expressions take the form of double integrals, they are based on extensions of the conventional integral which involve operations of both conventional integration and differentiation. In numerical computation the operation of differentiation can be a source of error, and so transformed versions of the familiar expressions are preferred in which the differentiation is applied directly to the known function, i.e. to the volume distribution or the lift distribution in the two cases concerned. If this is specified analytically, the differentiation can be carried out in closed form; if it is specified numerically, an approximation to the derivative, of an accuracy consistent with the data, can be obtained as a preliminary step. The calculation then involves summation processes only. The singularities are handled by the familiar techniques of a change of scale and the removal of the principal part, so that the evaluation is reduced to a double summation over a net of Gaussian points.

The leading edges the planform $y = \pm s(x)$, where x is measured downstream from the wing apex and y to starboard, are defined by expressing $s(x)$ as a polynomial in x. The trailing edges, being supersonic, do not appear explicitly in the calculation. All significant variations of planform in which the leading edge is smooth are covered by this formulation. The volume distribution of the wing is assumed to have a finite surface slope which varies continuously over the planform, except perhaps along the centre line, as is consistent with the limitation to sharp edges and smooth shapes. The load is assumed to vanish along the leading edges, in accordance with the assumption of attachment lines there, and to tend to zero like the square root of the distance from the edge. This is the familiar behaviour of closed form solutions for wings that have zero load along subsonic edges (*see* for instance, Refs. 15 to 18). The disturbance velocity potential corresponding to the lift distribution then behaves like $(1-\eta^2)^{2/3}$ near the leading edges, where $\eta = y/s(x)$. The further variation of the potential can then conveniently be represented by a double polynomial in x and η. It is suggested that this representation is superior to others in that lift distributions that combine low drag and attached flow arise simply and naturally from it.

The accuracy of the numerical analysis is investigated by a comparison of values computed by the programmes developed and some closed form results. Satisfactory agreement is obtained throughout except for very small values of βA—($\beta^2 = M^2 - 1$, M is the free-stream Mach number, A is the aspect ratio) and for points very near a sonic leading edge. These defects are explicable and, in any case, not relevant to the purposes for which the work was undertaken.

The adequacy of the linearized theory for the calculation of the pressure distribution on an unwarped wing at zero lift is shown by a comparison between values calculated by the present method and measured values. The design of a particular warped wing is described in some detail to illustrate the principles set

out above; the calculated mean surface is shown; and preliminary experimental results are quoted to indicate the success of the approach. Finally, an illustration is given of how the method of design can be adapted to deal with a configuration comprising a wing with a short, round fore-body.

2. *Discussion of Formulae.*

Within the linearized theory of supersonic flow past thin wings, the properties of a wing are separable into those of a wing which has the same distribution of volume, with top-and-bottom symmetry, at zero incidence, and of a wing which has the same mean surface (and so the same lift distribution) and no volume. Suppose the wing lies close to the plane $z = 0$ containing the free-stream direction ox and suppose that oy is measured to starboard with oz completing the right-handed rectangular system. Let the free-stream have speed U and Mach number M, with $\beta^2 = M^2 - 1$.

If the volume distribution of the wing corresponds to a streamwise surface slope $\pm\lambda(x,y)$ on the upper and lower surfaces of the wing respectively, the pressure coefficient C_p due to this volume distribution is given (*see* p.155 of Ref. 19, for instance) by

$$C_p(x,y) = -\frac{2}{\pi}\int dy_1 \int \frac{(x-x_1)\,\lambda(x_1,y_1)\,dx_1}{[(x-x_1)^2-\beta^2(y-y_1)^2]^{3/2}} \tag{1}$$

or

$$C_p(x,y) = \frac{2}{\beta}\lambda(x,y) - \frac{2}{\pi}\int dx_1 \int \frac{(x-x_1)\,\lambda(x_1,y_1)\,dy_1}{[(x-x_1)^2-\beta^2(y-y_1)^2]^{3/2}}. \tag{2}$$

Here, and subsequently in this section, the region of integration is that part of the planform lying in the Mach fore-cone of the point (x,y), i.e. the intersection of the regions $x_1 \geqslant 0$, $|y_1| \leqslant s(x_1)$ and $x_1 \leqslant x$, $\beta|y-y_1| \leqslant x-x_1$, as shown in Fig. 1. The notation $\int\!\!\!\!\!\!-\, f(x)dx$ denotes the 'finite part' of the integral. It is defined by

$$\int_a^x\!\!\!\!\!\!-\, \left(\frac{\partial}{\partial x}\right)^n \frac{A(x,y)\,dy}{\sqrt{x-y}} = \left(\frac{\partial}{\partial x}\right)^n \int_a^x \frac{A(x,y)\,dy}{\sqrt{x-y}}, \tag{3}$$

provided the expression on the right exists. From (1) and (3) follows the equivalent form

$$C_p(x,y) = \frac{2}{\pi}\frac{\partial}{\partial x}\iint \frac{\lambda(x_1,y_1)\,dx_1\,dy_1}{[(x-x_1)^2-\beta^2(y-y_1)^2]^{\frac{1}{2}}}. \tag{4}$$

If the distribution of lift over the wing corresponds to a local load coefficient $l(x,y)$ (equal to the difference in pressure coefficient between the lower and upper surfaces) and a difference $\Delta\phi(x,y)$ in velocity potential between lower and upper wing surfaces, the corresponding local incidence $\alpha(x,y)$ (equal to minus the streamwise slope of the mean surface) is given (*see* pp.156–7 of Ref. 19, for instance) by

$$\alpha(x,y) = -\frac{1}{4\pi}\int\!\!\!\!\!\!-\, dy_1 \int \frac{(x-x_1)\,l(x_1,y_1)\,dx_1}{(y-y_1)^2\,[(x-x_1)^2-\beta^2(y-y_1)^2]^{\frac{1}{2}}} \tag{5}$$

or

$$\alpha(x,y) = \frac{\beta}{4}l(x,y) - \frac{1}{4\pi}\int dx_1 \int\!\!\!\!\!\!-\, \frac{(x-x_1)\,l(x_1,y_1)\,dy_1}{(y-y_1)^2\,[(x-x_1)^2-\beta^2(y-y_1)^2]^{\frac{1}{2}}} \tag{6}$$

$$\alpha(x,y) = -\frac{\beta^2}{2\pi U}\int dy_1 \int \frac{\Delta\phi(x_1,y_1)\,dx_1}{[(x-x_1)^2-\beta^2(y-y_1)^2]^{3/2}} \tag{7}$$

or

$$\alpha(x,y) = \frac{\beta}{4}l(x,y) - \frac{\beta^2}{2\pi U}\int dx_1 \int \frac{\Delta\phi(x_1,y_1)\,dy_1}{[(x-x_1)^2-\beta^2(y-y_1)^2]^{3/2}}. \tag{8}$$

Here $\int\!\!\!\!\!\!-\, f(x)\,dx$ denotes the generalized principal value of the integral defined by the relation

$$n!\int\!\!\!\!\!\!-_a^b \frac{F(x,y)\,dy}{(y-x)^{n+1}} = \left(\frac{\partial}{\partial x}\right)^n \int_a^b \frac{F(x,y)\,dy}{y-x}, \tag{9}$$

where $a<x<b$, $F(x,y)$ has its first n derivatives with respect to x and y continuous at $y = x$, and the right-hand side is a Cauchy principal value.

The extra terms which arise in (2), (6) and (8) as compared with (1), (5) and (7) are due to the change in the order of integration. Equation (7) is obtainable from equation (5) by means of an integration by parts, when it is remembered that

$$l(x,y) = -\frac{2}{U}\frac{\partial}{\partial x}\Delta\phi(x,y). \tag{10}$$

If the characteristic coordinates u and v are introduced, where

$$Mx = \beta(u+v), \quad My = \beta(v-u),$$

equation (7) becomes

$$\alpha = -\frac{M}{8\pi U}\int\!\!\!\!\!\!-\int\!\!\!\!\!\!-\frac{\Delta\phi\,du_1\,dv_1}{(u-u_1)^{3/2}\,(v-v_1)^{3/2}}, \tag{11}$$

a symmetrical expression also quoted by Heaslet and Lomax. When the definition (3) is applied to equation (11), the result

$$\alpha = -\frac{M}{2\pi U}\frac{\partial^2}{\partial u\,\partial v}\int\int \frac{\Delta\phi\,du_1\,dv_1}{(u-u_1)^{\frac{1}{2}}\,(v-v_1)^{\frac{1}{2}}} \tag{12}$$

is obtained at once. This form has been used by Hancock[20].

Provided the known function l or $\Delta\phi$ is simple, a first integration in one or other of the equivalent formulae (5) to (8), (11), (12) can be carried out in terms of elementary functions; this is the case discussed by Roper[21]. In the present case the functions l and $\Delta\phi$ have branch points at the leading edges and the influence functions in the above equations all have branch points on the Mach lines; the result of a single integration therefore requires elliptic integrals, in general incomplete and of the third kind, for its expression. It is thought preferable, then, to perform both integrations numerically. The evaluation of (1) and (2) could begin with a first integration in terms of elementary functions if λ were specified simply, either over the whole wing or in the intervals of an interpolation scheme. However the technique evolved to deal with the lifting case proved so straightforward and accurate that it was adapted to treat the somewhat easier case of the symmetrical wing.

All the formulae quoted so far involve, either explicitly or by virtue of the definitions (3) and (9), the differentiation of functions which have to be calculated numerically. This is bound to be either slow or inaccurate relative to the integration processes and it also complicates the numerical analysis by the introduction of a further finite difference approximation with a truncation error independent of those in

the integration processes. If the order of the calculation can be inverted so that the differentiation operations are carried out directly on the data these difficulties disappear completely if the data is specified analytically. Even if the data is numerical the difficulties are removed from the main calculation and arise in the initial stage of preparing the derivatives of the data. Each case can then be given individual treatment and the significance to be expected of the results can be assessed. An example is given in Section 5.1 in which the accuracy was greater than had been expected.

If the leading edges are sharp and the volume distribution has smooth streamwise sections, as in the case considered here, it follows that the streamwise surface slope, λ, is finite at the leading edge and its derivative is well-defined and integrable in the Riemann sense. Manipulation of equation (4) then produces an equivalent result for the pressure coefficient due to the volume distribution:

$$C_p(x,y) = \frac{2}{\pi}\int_{Y_1}^{Y_2} \frac{\lambda(r(y_1),y_1)\,dy_1}{[(r-x)^2-\beta^2(y-y_1)^2]^{\frac{1}{2}}} + \frac{2}{\pi}\iint \frac{\partial\lambda(x_1,y_1)}{\partial x_1}\,\frac{dx_1\,dy_1}{[(x-x_1)^2-\beta^2(y-y_1)^2]^{\frac{1}{2}}} \tag{13}$$

where $x_1 = r(y_1)$ is the equation of the leading edges (i.e. $y \equiv s(r(y))$ if $y \geqslant 0$ and $y \equiv -s(r(y))$ if $y \leqslant 0$) and $Y_1(x,y)$ and $Y_2(x,y)$ are the intersections of the forward-going Mach lines from (x,y) with the port and starboard leading edges respectively (*see* Fig. 1). An expression of the same form as (13) has been given by Evvard (equation (42) of Ref. 22). The integration operations in equation (13) are conventional. For the subsequent numerical analysis it has been assumed that $\partial\lambda/\partial x_1$ is bounded, though the formula holds so long as it is integrable; there is then at worst just a pair of square root singularities at the end points of the range of integration and these are easily removed by the transformation introduced in the next Section.

If the lift distribution vanishes at the leading edges of the planform like the square root of the distance from the edge, both $\partial\Delta\phi/\partial u$ and $\partial\Delta\phi/\partial v$ vanish in the same way. Manipulation of equation (12) then leads to the equivalent result for the local incidence of the mean surface:

$$\alpha = -\frac{M}{2\pi U}\iint \frac{\partial^2\Delta\phi}{\partial u_1\,\partial v_1}\,\frac{du_1\,dv_1}{(u-u_1)^{\frac{1}{2}}(v-v_1)^{\frac{1}{2}}} \tag{14}$$

or, in the original coordinates:

$$\alpha(x,y) = \frac{1}{2\pi U}\iint \left(\frac{\partial^2\Delta\phi}{\partial y_1^2} - \beta^2\frac{\partial^2\Delta\phi}{\partial x_1^2}\right)\,\frac{dx_1\,dy_1}{[(x-x_1)^2-\beta^2(y-y_1)^2]^{\frac{1}{2}}}. \tag{15}$$

In equations (14) and (15) the integrations are conventional. The integrand has always a pair of square root singularities at the ends of the integration interval, whether these are points of the leading edges or points of the Mach lines. At the four corners of the curvilinear quadrilateral formed by the leading edges and the Mach lines these singularities coalesce and simple poles occur. These singularities are dealt with in the following Section by the classical methods. In the application to the design of the mean surface of a wing it is no effective restriction to require that $\Delta\phi$ be expressed analytically and the differentiations required by equations (14) or (15) can then be carried out in closed form.

On the other hand, since it is desirable to keep the expression for $\Delta\phi$ simple, the form of the expression chosen for it is important. In particular, it is desirable that distributions of lift which vanish along the leading edge and correspond to low lift-dependent drag should be simply expressible in the form chosen. To express the behaviour at the leading edges, given by $y = \pm s(x)$, in a natural form the coordinate $\eta = y/s(x)$ must be introduced. The upper-surface disturbance velocity potential $\phi = -\frac{1}{2}\Delta\phi$ then varies like $(1-\eta^2)^{3/2}$ near the leading edges, at which $\eta^2 = 1$. It is then more convenient to express the remaining variation of ϕ in terms of η and x, rather than y and x, since η is related to the planform shape. A polynomial in η^2, whose coefficients are polynomials in x, is chosen,

$$\frac{\phi(x,y)}{U} = -\frac{\Delta\phi}{2U} = (1-\eta^2)^{3/2}\sum_{n=0}^{N} a_n(x)\,\eta^{2n}, \tag{16}$$

$$a_n(x) = \sum_{m=1}^{M} b_{n,m}\,x^m, \tag{17}$$

so that ϕ is symmetrical about $\eta = 0$ and differentiable at $\eta = 0$. The leading edges are defined by a further polynomial

$$s(x) = \sum_{j=1}^{J} c_j\,x^j. \tag{18}$$

The constant terms are omitted from the sums in (17) and (18) to give a pointed planform and a finite local lift at the apex.

The simple case with $a_n(x) = b_{n,1}\,x$ now gives distributions of ϕ across the semi-span which are the same shape at all lengthwise stations. For a delta wing, this means the same distribution of lift and surface slope across the local semi-span at all lengthwise stations, i.e. conical camber. The application of conical camber is well known[23] to be a useful method of drag reduction for delta wings with subsonic leading edges. The inclusion of higher powers of x in $a_n(x)$ enables the lengthwise distribution of cross-loading,

$$L(x) = \int_{-s}^{s} \Delta C_p\,dy,$$

which determines the centre of pressure and which has a dominant effect on the lift-dependent wave drag when the leading edge is well subsonic, to be varied independently of the distribution of ϕ over the cross-sections. From (16), the lift $\bar{L}(x)$ on that part of the planform forward of the station x is given by

$$\bar{L}(x) = -\rho U\int_{-s}^{s} \Delta\phi\,dy = 4\rho\,U\,s(x)\int_{0}^{1} \phi(x,y)\,d\eta$$

$$= 3\pi\rho U^2\,s(x)\sum_{n=0}^{N}\frac{1\,.\,3\,.\,5\,\ldots\,.(2n-1)}{2^{n+1}(n+2)!}\,a_n(x), \tag{19}$$

provided the trailing edge is unswept. Then

$$L\,(x) = \frac{1}{q}\,\frac{d\bar{L}}{dx}.$$

If the conical behaviour near the wing apex expressed by (16) is excluded, for instance by expressing the local incidence as a double polynomial in x and y, the search for wings of low lift-dependent drag may lead to unnecessarily complicated shapes. Fig. 2, due to Germain and Fenain[24], shows the variation

in pressure coefficient, referred to overall lift coefficient, along the centreline of a delta wing with sonic leading edges. The absolute drag minimum for this case was determined by Germain[25], and the corresponding pressure distribution is shown, labelled 'optimum', The other pressure distributions are for wings which are optima within limited families, the size of the families increasing with the parameter N. The conical solutions, with finite pressure on the centreline at the apex and lengthwise loading varying like x near the apex, are not included in the families, so that the convergence as $N \to \infty$ is non-uniform and the unfavourable pressure gradients steepen as N increases.

This same example provides further support for the present approach of seeking a lifting surface of low drag by semi-empirical means, rather than by an entirely mathematical optimization process. The lift-dependent drag associated with the $N = 5$ restricted optimum is only 4 per cent above the absolute minimum (*see* Fig. 46 of Ref. 26). Similarly, the conical solutions of Smith and Mangler[23] gave a drag only 5 per cent above the absolute minimum for the case of sonic leading edges. These figures are small compared with the discrepancies commonly observed between measured and calculated lift-dependent drags. Therefore a lift distribution which may differ substantially from a theoretically determined optimum, but which is attainable in a real flow, may well lead to a wing of lower measured lift-dependent drag than a lift distribution which is theoretically an optimum. This conclusion is reinforced if the theoretical optimum is obtained within a class which may be inappropriately restricted.

The next two sections of this paper deal with the details and the accuracy of the procedures for evaluating the expressions in equations (13) and (15). Examples of the application of these procedures are given in Section 5.

3. *Numerical Analysis.*

The right-hand side of the equation for the pressure due to the volume distribution of the wing, equation (13), consists of two terms. The single integral is clearly more straightforward to evaluate than the double integral and this in turn is simpler than the double integral in equation (15) because $\partial\lambda/\partial x$ has been assumed to be bounded. It is the evaluation of the right-hand side of equation (15), for the local incidence associated with a given lift distribution that will be considered in detail; the reader interested in treating the symmetrical wing only can omit the unnecessary refinements*.

Note first that the partial derivatives with respect to x_1 and y_1 in equation (15) are for y_1 and x_1 constant, respectively, but that ϕ is given by equation (16) in terms of x_1 and η. The relevant relations are

$$\frac{\partial^2\phi}{\partial x_1^2} = \frac{\partial^2\phi}{\partial x_1^2} + 2\frac{\partial^2\phi}{\partial\eta\,\partial x_1}\frac{\partial\eta}{\partial x_1} + \frac{\partial\phi}{\partial\eta}\frac{\partial^2\eta}{\partial x_1^2} + \frac{\partial^2\phi}{\partial\eta^2}\left(\frac{\partial\eta}{\partial x_1}\right)^2$$

$$\frac{\partial^2\phi}{\partial y_1^2} = \frac{\partial^2\phi}{\partial\eta^2}\left(\frac{\partial\eta}{\partial y_1}\right)^2$$

where the derivatives with respect to x_1 are for y_1 constant on the left and for η constant on the right. The derivatives of η are immediate:

$$\eta = \frac{y_1}{s(x_1)}, \quad \frac{\partial\eta}{\partial y_1} = \frac{1}{s(x_1)}$$

$$\frac{\partial\eta}{\partial x_1} = -\frac{\eta s'}{s}, \quad \frac{\partial^2\eta}{\partial x_1^2} = \eta\left(\frac{2s'^2}{s^2} - \frac{s''}{s}\right).$$

With these substitutions it is clear that

---

*But *see* the last paragraph of the Section.

$$\frac{1}{U}\left\{\frac{\partial^2\Delta\phi}{\partial y_1^2}-\beta^2\frac{\partial^2\Delta\phi}{\partial x_1^2}\right\}=\frac{2P(x_1,\eta)}{(1-\eta^2)^{\frac{1}{2}}}, \tag{20}$$

where $P(x_1,\eta)$ is a polynomial in η^2. The coefficients of this polynomial are rational functions of x_1, which are bounded except for a simple pole at $x_1 = 0$. This pole is cancelled by the factor $s(x_1)$ introduced into the numerator of the integrand of (15) by the change of variable $dy_1 = s(x_1)\,d\eta$. The denominator of the integrand of (15) can be written

$$\left[\left(x-x_1\right)^2-\beta^2\left(y-y_1^2\right)\right]^{\frac{1}{2}}=\beta s(x_1)\,(\eta-\eta_1)^{\frac{1}{2}}(\eta_2-\eta)^{\frac{1}{2}},$$

where

$$\left.\begin{aligned}\eta_1=\eta_1(x_1)&=-\frac{x-x_1-\beta y}{\beta s(x_1)}\\ \text{and}\qquad\\ \eta_2=\eta_2(x_1)&=\frac{x-x_1+\beta y}{\beta s(x_1)}\end{aligned}\right\} \tag{21}$$

This term remains non-zero as $x_1\to 0$ for fixed x and y, so no singularity is introduced at the apex. The lines $\eta=\eta_1(x_1)$ and $\eta=\eta_2(x_1)$ are the Mach lines through (x,y), as shown in Fig. 1. When (20) and (21) are substituted into (15) it becomes

$$\alpha(x,y)=\frac{1}{\beta\pi}\iint\frac{P(x_1,\eta)\,d\eta\,dx_1}{(1+\eta)^{\frac{1}{2}}(1-\eta)^{\frac{1}{2}}(\eta-\eta_1)^{\frac{1}{2}}(\eta_2-\eta)^{\frac{1}{2}}}. \tag{22}$$

The integrand has been put into this form with a view to carrying out the integration with respect to y_1 or η first; this choice of the order of integration reduces the number of times the leading edge equation $y_1 = s(x_1)$ has to be solved for x_1 in the course of the calculation. The second integration, that with respect to x_1, extends from $x_1 = 0$ to $x_1 = x$ and in this range the end-points of the interval of the first integration change their form. Suppose the pivotal point (x,y) is in the starboard half-wing ($y>0$), as in Fig. 1. Let the left-hand forward-going characteristic through (x,y) meet the port leading edge where $x_1=\bar{x}_1$, $y_1=-s(\bar{x}_1)$, $\eta=\eta_1(\bar{x}_1)=-1$. Then for $0\leqslant x_1\leqslant\bar{x}_1$, the η-integration is over the range $(-1, 1)$. Call this Region I of the wing. Let the right-hand forward-going characteristic through (x,y) meet the starboard edge where $x_1=\bar{x}_2$, $y_1=s(\bar{x}_2)$, $\eta=\eta_2(\bar{x}_2)=1$. Then for $\bar{x}_1\leqslant x_1\leqslant\bar{x}_2$ the η-integration is over the range $(\eta_1, 1)$ and this is called Region II. The remaining range, $\bar{x}_2\leqslant x_1\leqslant x$ is called Region III, with the η-integration over the interval (η_1, η_2).

Each integration with respect to η in equation (22) is between two square-root singularities of the integrand and two further square-root singularities occur outside the range of integration, unless $x_1=\bar{x}_1$ or $\bar{x}_2$. For these two special values of x_1, the integrand has a pole, since $\eta_1(\bar{x}_1)=-1$ and $\eta_2(\bar{x}_2)=1$. The first step is to remove the principal parts at these poles. Since, when $y=0$, Region II disappears and $\bar{x}_1=\bar{x}_2$, both poles must be dealt with in all three Regions. Consider Region I first. In equation (22) $P(x_1,\eta)$ is replaced by

$$\bar{P}(x_1,\eta)=P(x_1,\eta)-P(\bar{x}_1,-1)\sqrt{\frac{1-\eta}{1-\eta_1}\,\frac{\eta_2-\eta}{\eta_2-\eta_1}}-P(\bar{x}_2,1)\sqrt{\frac{1+\eta}{1+\eta_2}\,\frac{\eta-\eta_1}{\eta_2-\eta_1}} \tag{23}$$

and the corresponding additional terms

$$P(\bar{x}_1,-1)\int_0^{\bar{x}_1}\frac{dx_1}{\sqrt{(1-\eta_1)(\eta_2-\eta_1)}}\int_{-1}^{1}\frac{d\eta}{\sqrt{(1+\eta)(\eta-\eta_1)}} \tag{24}$$

$$P(\bar{x}_2,1)\int_0^{\bar{x}_1}\frac{dx_1}{\sqrt{(1+\eta_2)(\eta_2-\eta_1)}}\int_{-1}^{1}\frac{d\eta}{\sqrt{(1-\eta)(\eta_2-\eta)}} \tag{25}$$

are added. The terms subtracted from $P(x_1,\eta)$ are not the simplest that could have been chosen; they have the advantage that the η-integrals in (24) and (25) are expressible in elementary functions. The integrand is treated in a similar fashion in Regions II and III, as displayed in Appendix A.

The treatment of the six terms like (24) and (25) which arise from the three Regions can be exemplified by that of (24). The η-integration is elementary:

$$\int_{-1}^{1}\frac{d\eta}{\sqrt{(1+\eta)(\eta-\eta_1)}}=2\log\frac{\sqrt{2}+\sqrt{1-\eta_1}}{\sqrt{-1-\eta_1}}. \tag{26}$$

Now, by equation (21)

$$-1-\eta_1=\frac{x-x_1-\beta y-\beta s(x_1)}{\beta s(x_1)}=\frac{(\bar{x}_1-x_1)\,Q(x_1)}{\beta s(x_1)}$$

where $Q(x_1)$ is a polynomial in x_1, since $s(x_1)$ is a polynomial and $\eta_1(\bar{x}_1). = -1$. Thus (24) becomes

$$P(\bar{x}_1,-1)\int_0^{\bar{x}_1}\log\frac{\beta s(x_1)(\sqrt{2}+\sqrt{1-\eta_1})^2}{Q(x_1)}\,\frac{dx_1}{\sqrt{(1-\eta_1)(\eta_2-\eta_1)}}-$$

$$-P(\bar{x}_1,-1)\int_0^{\bar{x}_1}\log(\bar{x}_1-x)\frac{dx_1}{\sqrt{(1-\eta_1)(\eta_2-\eta_1)}}. \tag{27}$$

The integrand of the first term is finite throughout the range, and its indeterminacy at $x_1 = 0$ is irrelevant, since the integration formula to be used does not require values of the integrand at end-points of the range. The integrand of the second term in (27) has a logarithmic singularity at $x = x_1$ which is readily removed:

$$\int_0^{\bar{x}_1}\log(\bar{x}_1-x)\frac{dx_1}{\sqrt{(1-\eta_1)(\eta_2-\eta_1)}}=\int_0^{\bar{x}_1}\log(\bar{x}_1-x_1)\left\{\frac{1}{\sqrt{(1-\eta_1)(\eta_2-\eta_1)}}-\frac{1}{\sqrt{2(\eta_2(\bar{x}_1)+1)}}\right\}dx_1$$

$$+\frac{\bar{x}_1(\log\bar{x}_1-1)}{\sqrt{2(\eta_2(\bar{x}_1)+1)}}. \tag{28}$$

The integrand on the right of equation (28) is finite throughout the range. Thus expression (24) has been reduced to a sum of elementary functions and of single integrals of finite functions. Expression (25) and

the four similar expressions from Regions II and III are dealt with similarly. Appendix A shows the result.

The remaining term is the double integral which arises when $\bar{P}$ is written for P in equation (22), viz.

$$\iint \frac{\bar{P}(x_1,\eta)\, d\eta\, dx_1}{(1+\eta)^{\frac{1}{2}}(1-\eta)^{\frac{1}{2}}(\eta-\eta_1)^{\frac{1}{2}}(\eta_2-\eta)^{\frac{1}{2}}} \tag{29}$$

where $\bar{P}(x_1,\eta)$ is defined by equation (23). The integrand now has a square-root singularity at each end of the range of integration with respect to η for every value of x_1 except $x_1 = \bar{x}_1$ and $\bar{x}_2$. For these values it vanishes at one end of the range. These singularities can be removed to a fixed distance beyond the range of integration by a simple transformation of η. Again consider Region I, where the singularities are at $\eta = \pm 1$. Let

$$\eta = \frac{1}{2}\xi(3-\xi^2), \quad -1 \leqslant \xi \leqslant 1. \tag{30}$$

Within this ξ-interval the transformation is one-to-one and the intervals $(-1, 1)$ correspond (*see* Fig. 3). It is found that

$$\frac{d\eta}{\sqrt{1-\eta^2}} = \frac{3d\xi}{\sqrt{4-\xi^2}}, \tag{31}$$

so that expression (29) becomes, in Region I,

$$\int_0^{\bar{x}_1}\int_{-1}^{1} \frac{\bar{P}(x_1,\eta(\xi))\, 3d\xi\, dx_1}{(2-\xi)^{\frac{1}{2}}(2+\xi)^{\frac{1}{2}}(\eta(\xi)-\eta_1)^{\frac{1}{2}}(\eta_2-\eta(\xi))^{\frac{1}{2}}}. \tag{32}$$

The integrand is now non-singular throughout and the branch points (which cannot be eliminated by an algebraic transformation) are removed from the range. Similar transformations are given in Appendix A for Regions II and III. The transformation

$$\eta = \sin\frac{\pi\xi}{2}, \quad -1 \leqslant \xi \leqslant 1$$

would serve as well as (30), which was preferred for speed of computation.

The double integral on the right of equation (22) has now been expressed as the sum of three double integrals, a number of single integrals and some elementary functions; all the integrands are bounded on the respective regions of integration. Gaussian integration is now employed to evaluate the local incidence. In each region the 10-point formula is applied in both directions, i.e. the ten Gaussian points are distributed in the ranges $(0, \bar{x}_1)$, $(\bar{x}_1, \bar{x}_2)$ and $(\bar{x}_2, x)$ and at each of these 30 values of x_1 the ten Gaussian points are distributed in the range $(-1, 1)$ to form the values of ξ. These values of ξ are used to form η, using equation (30) or the corresponding expressions in Appendix A. The integrand of (32) follows using (16), (17), (18), (20) and (23). Approximations to expression (32) and the two similar ones for Regions II and III follow by summation. The integrands of the single integrals are then evaluated and a final summation in the x-direction performed. The complete expression and the necessary transformations are written out in full in Appendix A.

The calculation described has been programmed for the Ferranti 'Mercury' electronic computer, using Autocode. It is not thought worthwhile to reproduce a flow diagram of the programme, since the calcu-

lation, though complicated, is entirely straightforward. All the quantities required can be determined in order from the equations given and the only additional information a flow diagram could supply would be the division of the programme into chapters*.

With 100 coefficients $b_{n,m}$ in the expressions (16) and (17) for ϕ, the programme takes between four and five minutes to calculate the local incidence at a point. With only a few coefficients, the time is reduced to between 2 and $2\frac{1}{2}$ minutes. Obviously a large proportion of the time is being spent on the evaluation of the derivatives of ϕ, the function $P(x_1,\eta)$ being evaluated at 300 points of the planform. In order to define the mean surface of the wing, the local incidence is needed at about 100 points, so that in the course of such a calculation $P(x_1,\eta)$ would be found at about 3×10^4 points. Time would be saved therefore (neglecting access time) if values of $P(x_1,\eta)$ were stored in a table of 10^4 entries with subsequent interpolation. Fortunately it is unnecessary to balance access time against computing time because a table of about 10^2 entries turns out to provide adequate accuracy and such a table can be accommodated in the high speed store of Mercury.

The scheme used is to compute the values of $x_1\,P(x_1,\eta)$ for $\eta^2 = -0{\cdot}1(0{\cdot}1)1$ and $x_1 = -0{\cdot}1\ (0{\cdot}1)1$** on first entering the programme and then, when a value of $P(x_1,\eta)$ is subsequently called for, to interpolate for it using a second-order backward-difference formula in two variables. $x_1\,P(x_1,\eta)$ is chosen as the argument of the table since it remains finite everywhere and η^2 is chosen as an independent variable in preference to η since with equal intervals it covers the spanwise variation better. If the relation of the point (x, η^2) to the neighbouring tabular points is as illustrated in Fig. 4, the appropriate formula is

$$\begin{aligned}
4h^4 f &= 4h^4\, x_1\, P(x_1,\eta) \\
&= \delta\varepsilon(h-\delta)\,(h-\varepsilon)f_0 - \delta\varepsilon(h+\delta)\,(h-\varepsilon)f_2 \\
&\quad - \delta\varepsilon(h-\delta)\,(h+\varepsilon)f_6 + \delta\varepsilon(h+\delta)\,(h+\varepsilon)f_8 - 2\varepsilon(h-\varepsilon)\,(h^2-\delta^2)f_1 \\
&\quad - 2\delta(h-\delta)\,(h^2-\varepsilon^2)f_3 + 2\delta(h+\delta)\,(h^2-\varepsilon^2)f_5 + 2\varepsilon(h+\varepsilon)\,(h^2-\delta^2)f_7 \\
&\quad + 4(h^2-\delta^2)\,(h^2-\varepsilon^2)f_4. \qquad (33)
\end{aligned}$$

Using this alternative programme to calculate the local incidence reduces the time taken for each point after the first to about 40 seconds. The loss in accuracy is small and, in the present context, entirely acceptable. This can be seen from the following Section, where comparisons are given of results using the two programmes (with and without tabular interpolation) with results derived independently.

Before proceeding to these comparisons, it is convenient to mention here how the ordinates of the mean surface have been obtained from the values of the local incidence. The local incidence is calculated for $x = 0(0{\cdot}1)1$ and $\eta = 0(0{\cdot}1)1$ by the programme described above. (In fact, the programme fails for $x = 0$, $\eta = 0$ and $\eta = 1$ due to the complete collapse of one or more of the Regions I, II, III, so values of x and η slightly different from these are used.) A formula like equation (33) is then used to obtain values of α at intermediate points. For this, an additional row and column are required in the table, obtained by putting

$$\alpha|_{\eta=-0{\cdot}1} = \alpha|_{\eta=0{\cdot}1},$$

in accordance with the symmetry of the wing, and

---

*A 'chapter' is the block of instructions occupying the high speed store at any one time. The programme contained six of them. This is only relevant to Mercury: readers wishing to perform these calculations on Mercury or compatible computers should write to the first author.

**To avoid the need to programme the limiting form of $x_1\,P(x_1,\eta)$ for $x_1 = 0$ separately, a small number is used in place of 0.

$$\alpha|_{x=-0\cdot1} = 2\alpha|_{x=0} - \alpha|_{x=0\cdot1},$$

an arbitrary choice affecting a small region of the wing only. The ordinate, $z(x,y)$, of the mean surface is determined by the relation

$$\frac{\partial z}{\partial x} = -\alpha(x,y);$$

together with an initial value $z(x_c(y),y) = f(y)$, normally chosen to give straight hinge-lines for control surfaces. The interval $x<x_1<1$ on the line $y_1 = y$ is divided into 5 equal intervals and in each of these 10 Gaussian integration points are taken. The approximate value of z then follows by summation, with the appropriate weights, of the corresponding values of α obtained by tabular interpolation. A constant number of points rather than a constant integration interval was chosen partly for simplicity and partly to obtain sufficient accuracy in the important wing-tip region without disproportionate effort elsewhere. The large number of integration points relative to the small number of tabular points appears inconsistent. However, the final shape arrived at must be smooth to a high order of accuracy, whereas it need only correspond to the exact shape as predicted by linear theory to an order closer than the predictions of the theory are likely to correspond to a real flow. For instance, on a model five feet long, the ordinates must be smooth to within 0·001 inch, but the predictions of linear theory are unlikely to be significant to more than 0·1 inch, so if the ordinates agree with linear theory to within 0·01 inch the possible sources of error are adequately distinguished.

At the opening of this section the problem of calculating the surface pressure due to the wing volume distribution was dismissed as relatively easier than the calculation of local incidence. However, two additional complications do arise. The more important concerns the specification of the volume distribution. Since this must be chosen to provide the required stowage space, with enough thickness to provide strength and rigidity in a light structure, all at the least possible cost in drag, it is unlikely that it can be specified in terms which the programmer has chosen in advance. Two cases arise; in the first, an analytic representation is possible but exceedingly complicated; in the second it cannot be attempted. The procedure in the second case is described in Section 5.1. In the first case, typified by the wing reported on by Courtney and Ormerod[27], whose shape is given by Clark[28], the difficulty lies in the formation and calculation of the second derivatives of a very complicated function. Here it has been found helpful to programme the usual formulae for the derivatives of the functions which arise, as explained in Appendix B. In both the first and second cases the calculation of $\lambda(x,y) = \partial z/\partial x$ and $\partial\lambda/\partial x$ for use in equation (13) must be by means of a sub-programme which can be replaced as a whole. The second, and minor, complication is that, in order to deal with the familiar case of the wing with diamond cross-sections, provision must be made for the presence of a ridgeline along the centreline of the wing. This means that the regions of integration shown in Fig. 1 must be subdivided along the centreline, so that the numerical integration formula is appropriate to the behaviour of the integrand within each region. The two cases illustrated in Fig. 5 then arise, depending on the point of the planform at which the pressure is required. Since there are now either 6 or 7 regions instead of 3, considerations of high-speed store capacity and computing time make it advisable to choose fewer integration points in each region. It appears from the results that an array of 7×7 Gaussian points in each region is adequate, so the programme allows for 7 or fewer points, the latter being useful for checking the accuracy.

4. *Accuracy of Methods.*

The adequacy of the numerical analysis of the previous Section can only conveniently be assessed by making comparisons between calculations by the programmes described and independently calculated results of linearized theory for the relatively simple cases that can be treated in closed form. Perhaps inevitably, such comparisons can never be completely convincing, in as much as they are made for simpler cases than those for which the calculation procedure is intended. In the end, some of the confidence generated

in the techniques arises from the self-consistency of the results and a little, in a completely illogical fashion, from their empirical success described in Section 5.

4.1. *Accuracy of the Calculated Pressure Distribution.*

To test the adequacy of the numerical analysis and the accuracy with which it has been programmed in the case of the calculation of the pressure due to a distribution of volume, consider a delta wing with the so-called Lord V area distribution and diamond cross-sections. Pressure distributions at two spanwise stations were calculated for this wing by Eminton[29], who performed one intergration analytically and one numerically, and confirmed by Firmin[30], who obtained a result in closed form. For a wing of length c, semi-span s_T and centreline thickness to chord ratio 0·1123, at a Mach number such that $\beta s_T/c = 3^{-\frac{1}{2}}$, the pressure at the points whose coordinates relative to the apex are quoted is

y/s_T	x/c	C_p *(present method)*	C_p *(Eminton)*
0·05	0·1	0·1504	0·1504
	0·2	0·0396	0·0396
	0·3	−0·0205	−0·0209
	0·5	−0·0711	−0·0710
	0·7	−0·0761	−0·0764
	0·9	−0·0694	−0·0694
0·575	0·6	0·0075	0·0069
	0·7	−0·0601	−0·0603
	0·9	−0·0827	−0·0827

The agreement demonstrated, even close to the leading edge, is entirely adequate for the purposes for which the calculation method was developed. The maximum error of 0·0006 is less than 1 per cent of the peak suction on the wing, whereas differences between linear theory and experiment commonly exceed 10 per cent. On the thicker wings, such as those studied by Cooke[31], this may be ascribed to second order effects of the inviscid flow; on thinner wings the pressures induced by boundary layer growth form a larger proportion of the total pressure.

4.2. *Accuracy of the Calculated Warp Distribution.*

For the calculation of the warp of the mean surface required to induce a specified distribution of lift, three test cases are presented. The errors are to be judged against the standard of a deviation of 1 per cent of the maximum slope of the mean surface, proposed to keep the errors in approximating to the 'exact' linear theory an order of magnitude smaller than the discrepancies arising from use of the linear theory. In each case two versions of the present calculation are given: one using the full method involving the direct evaluation of $P(x_1,\eta)$ [equation (20)] at each integration point and the other using the time-saving version in which values of P are obtained by interpolation.

(a) The simplest test case is that of a delta wing with the simplest conical camber that provides the appropriate behaviour of the load near the leading edges. From Ref. 23 it can be found that if

$$l = 4(1+2\eta^2)(1-\eta^2)^{\frac{1}{2}}$$

so that

$$\frac{\phi}{U} = x(1-\eta^2)^{3/2}$$

then

$$\alpha = -\frac{w}{U} = \frac{1}{\beta^2 K^3}\left\{\beta^2 K^2 K'(\beta K) - (2-\beta^2 K^2) E'(\beta K) + 2(1-\beta^2 K^2 \eta^2)^{3/2}\right\} \tag{34}$$

where $y = s(x) \equiv Kx$ is the starboard leading edge and E' and K' are the complete elliptic integrals of complementary modulus. With $K = 1$, α is a function of β and η only and the following values are found:

β	η	α (*full version*)	α (*with interpolation*)	α [*equation* (34)]
1	0·50	1·299	1·299	1·299
1	0·80	0·431	0·431	0·432
1	0·95	0·078	0·078	0·061
1	0·99	−0·028	−0·028	0·006
0·5	0·95	−0·869	−0·869	−0·869
0·5	0·99	−1·068	−1·068	−1·073
0·1	0·50	0·762	0·762	0·763
0·01	0·50	0·616	0·616	0·750

From these values it can be seen that the required accuracy is not obtained very near the leading edge of a sonic-edged delta wing, nor for very small values of βK. In both cases this is explicable in terms of the extreme shapes which Regions I, II and III adopt (*see* Fig. 1). The programme is not intended for these cases: at the other calculated points the agreement is well within 1 per cent of the maximum incidence. The agreement of the two versions of the programme is not surprising, since for this very simple case the interpolation formula is exact.

(b) Another fairly simple, but non-conical, case is given by Roper[16]. For a delta wing with $K = 0{\cdot}6$ and $\beta = 1$, the local incidence

$$\alpha = 3{\cdot}57908\, y^2 x^3 - 10{\cdot}89721\, y^4 x \tag{35}$$

corresponds to a local load distribution

$$l = x^5(0{\cdot}207177 + 2{\cdot}42346\,\eta^2 - 0{\cdot}631764\,\eta^4)(1-\eta^2)^{\frac{1}{2}}$$

and so to a distribution of potential

$$\frac{\phi}{U} = x^6(0{\cdot}00863237 + 0{\cdot}157941\,\eta^2)(1-\eta^2)^{3/2}.$$

For this case the comparable values of α are:

x	y	α (*full version*)	α (*with interpolation*)	α (*equation* (35))
0·34	0·2	−0·0003010	−0·0003034	−0·0003012
0·40	0·2	0·002187	0·002285	0·002188
0·60	0·2	0·02046	0·02078	0·02046
1·00	0·2	0·12570	0·1263	0·12573

The full version of the programme is extremely accurate, even close to the leading edge. The loss of accuracy in using interpolation is still within the limit of 1 per cent of the maximum value of α on the wing.

(c) Wings with curved subsonic leading edges are not amenable to exact treatment by linear theory. However, the not-so-slender theory of Adams and Sears[32] has been applied to them by Squire[33], and this provides an approximation to linear theory with which the present approximation can be compared.

Unfortunately, as was seen above, the present treatment involves an increasing error as $\beta \to 0$, while it is only in this limit that the not-so-slender theory is exact. The so-called 'gothic' planform

$$s(x) = 0{\cdot}25\, x\,(2-x) \qquad 0 \leqslant x \leqslant 1$$

is suitable simple. Then to the potential distribution

$$\frac{\phi}{U} = 0{\cdot}25\, x\,(2-x)\,(1-\eta^2)^{3/2}$$

corresponds the expression

$$\alpha = 1{\cdot}5 - 3\eta^2 + \frac{\beta^2}{256}\left(9 + 8\eta^4 + 12 \log \frac{\beta}{16}\right) \tag{36}$$

for the local incidence at the trailing edge $x = 1$, according to not-so-slender wing theory. This yields the comparison, for $\beta = 0{\cdot}2$ and $x = 1$:

y	α (*full version*)	α (*with interpolation*)	α (*equation* (36))
0·05	1·368	1·364	1·373
0·10	1·008	1·005	1·013
0·15	0·409	0·407	0·413
0·20	−0·430	−0·432	−0·426
0·24	−1·272	−1·273	−1·271

For this value of β the two approximations to linear theory agree to within the desired accuracy and the use of interpolation does not upset this conclusion. The agreement of the two approximations may, of course, be coincidental, but it tends to increase confidence in the present programme.

From these three examples it is concluded that the full method agrees well enough with the exact linear theory in the sort of case for which it was intended and that the loss of accuracy resulting from the use of interpolation is acceptable.

5. *Application of Methods.*

5.1. *Calculation of the Pressure Distribution Over an Unwarped Wing at Zero Lift.*

For the example to be discussed here, the ordinates $z(x,y)$ of the upper surface of the unwarped wing were specified numerically at the points of a rectangular lattice covering the planform. The sub-programmes to calculate the values of $\partial\lambda/\partial x = \partial^2 z/\partial x^2$ at points of the planform and values of $\lambda = \partial z/\partial x$ along the leading edge were therefore constructed to use linear interpolation in tables of these quantities to be provided as data for the computer. The proper way to obtain these data from the ordinates supplied is to use a combination of formal and intuitive methods to give a set of values of $\partial\lambda/\partial x$ which can be re-integrated to give the original ordinates to within manufacturing tolerances and are at the same time as smooth as possible. This is a formidable task, so two preliminary methods were tried. For the first, the requirement that the original ordinates could be recovered was dropped and a rather arbitrarily smoothed set of values of $\partial\lambda/\partial x$ was used for the calculation. For the second, the requirement of smoothness was dropped and the second differences of the ordinate values, extrapolated to the planform edges, were used. These are shown in Table 1, with the values of λ along the leading edge, required for the first integral of equation (13), in Table 2. It is clear that the values of $\partial\lambda/\partial x$ are not smooth and many apparently unsystematic variations appear. However, the pressure distribution calculated from the 'smooth' values of $\partial\lambda/\partial x$ showed irregularities very similar to those in the distribution calculated from values of $\partial\lambda/\partial x$ obtained by differencing; but the levels of pressure reached were somewhat different. Accordingly, the

calculations based on the unsmoothed differences were preferred, as being more likely to give the pressure levels correctly, whatever the significance of the irregular variations.

The planform of the wing is shown in Fig. 6, with the lattice of points at which $\partial\lambda/\partial x$ was specified on the left-hand side. On the right-hand side are shown the stations at which Taylor[8] measured pressures on a model of the wing. Some cross-sections of the wing are drawn in Fig. 7 and arranged to give a foreshortened view of the model. The measured and calculated pressures at a Mach number of 2·2 and a Reynolds number of 15 million (based on centreline chord) are shown in Fig. 8.

The agreement is, in fact, rather better, in terms of the peak suction on the wing, than that reported by Cooke[31] on a delta wing with diamond cross-sections and Lord V area distribution, for which the linear theory has been obtained in closed form[30]. The explanation for this is probably that Taylor's wing is somewhat thinner: centreline thickness to chord ratio of 0·055 as against 0·112 and (volume)/(plan area)$^{3/2}$ of 0·0415 as against 0·0519. In any case the agreement gives confidence in the use of the method, even when the data seem unpromising.

5.2. *The Design of an Efficient Trimmed Lifting Surface.*

The considerations governing the choice of a lift distribution for a slender wing at its attachment incidence have been set out in general terms in the introduction. Their application to a particular case will now be described in more detail.

The planform of the wing for which a warp distribution is required is shown in Fig. 9. The wing is intended to cruise at $M = 2{\cdot}2$ at $C_L = 0{\cdot}1$ without control surface deflections and with a centre of gravity position giving neutral longitudinal static stability under the approach conditions of $M \simeq 0{\cdot}2$, $C_L \simeq 0{\cdot}5$. On the basis of the arguments of the introduction, the leading edges are to be attachment lines at $C_L = 0{\cdot}05$ at $M = 2{\cdot}2$. In the absence of tests on this particular planform, the aerodynamic centre under the approach conditions was taken from a correlation with centre-of-area position originating with Messrs. Handley-Page Ltd. and given in Ref. 2. The centre of area is at 68·7 per cent of the length from the apex; the corresponding aerodynamic-centre position is at 64·7 per cent of the length from the apex; and the centre of gravity is supposed to be at the same point. Since the lift distribution is being specified at a lift coefficient different from the cruise, the aerodynamic centre under cruising conditions is also needed. Again in the absence of tests, an empirical estimate given in Ref. 2 was employed. It appears that the aerodynamic centre of a slender wing under approach conditions is some 7 to 8 per cent of its length forward of the aerodynamic centre at $M \simeq 2$, $C_L \simeq 0{\cdot}1$. With the higher value, this means that the centre of pressure at $C_L = 0{\cdot}05$, $M = 2{\cdot}2$ must be 16 per cent of the length ahead of the aerodynamic centre, i.e. 8 per cent ahead of the centre of gravity or 56·7 per cent of the length from the apex. This is the requirement for trim.

The requirement for efficiency, i.e. for a low drag due to lift at cruise, is harder to formulate, since the effect on drag of the flow separation from the leading edge is only qualitatively understood. The division of the drag into wave drag and vortex drag on the basis of the transport of momentum across a distant control surface can still be made, but these can no longer be connected with the lift distribution over the wing, as is possible when the flow is attached. However, in the choice of the lift distribution for low drag it was assumed that the drag could be divided into two parts, one of which again depends on the spanwise distribution of chord loading and is independent of Mach number and another which depends mainly on the lengthwise distribution of cross-loading (*see* Section 2) at the cruising condition.

Calculations of vortex drag in attached flow show that low values can be obtained with spanwise distributions of chord loading which arise, according to slender thin-wing theory, from wings with a flat central part and leading-edge regions drooped outboard of a 'shoulder-line' (Weber[15]). As the point where the shoulder-line meets the trailing edge approaches the wing tip, the vortex drag tends to the theoretical minimum and the pressure gradients on the wing increase. A compromise that seems obtainable in a real flow is reached with a 'shoulder-line' 75 per cent of the semi-span from the centreline, when the vortex drag is less than 10 per cent above the minimum. The corresponding chord loading is shown in

Fig. 10a. Experiment shows that wings of this form have drag factors* which decrease as the lift coefficient increases above that for attached flow, at all Mach numbers for which the flow separates from the leading edge. Hence a chord-loading distribution of this kind was specified for the wing to be designed in the hope of achieving a low value of the first component of the lift-dependent drag. The one chosen is also shown in Fig. 10a.

The remainder of the lift-dependent drag has been assumed to depend mainly on the lengthwise distribution of cross-loading, just as the lift-dependent wave drag does, to the first order in βA, in attached flow. At the cruising condition the cross-loading distribution must give the centre of pressure at the centre of gravity. From calculations made for attached flow, it is thought that for low drag the peak value of the cross-loading should be as low as possible and the cross-loading at the trailing edge should be substantial. Moreover, a smooth distribution is desirable if the design load is to be achieved in a real flow. Fig. 10b shows the lengthwise distribution of cross-loading that emerged from these considerations. From this must be subtracted the lengthwise distribution of cross-loading corresponding to incidence, which in general could be obtained from measurements of pressures on a model or from a calculation by linear theory, but which was in this case estimated from a combination of measurements and theory for different planforms. This leaves the lengthwise load distribution at the attachment incidence as shown in Fig. 10b, with its centre of pressure at the required station, 56·7 per cent of the length from the apex.

The distribution of chord-loading shown in Fig. 10a is equally the distribution of ϕ/U along the trailing edge. If a similar distribution were chosen at all lengthwise stations, the distribution of local lift across the local semi-span would be peaky at all lengthwise stations and all cross-sections of the mean surface part of the unwarped wing are superimposed on such a mean surface the resulting wing shape appears would be drooped fairly sharply near the leading edge. When the thick cross-sections of the forward unlikely to encourage an orderly development of separated flow originating from a single separation line along the leading edge. Accordingly, the distribution of ϕ/U across the local semi-span is modified gradually towards the apex of the wing, so that pressure gradients are reduced and the typical cross-section of the mean surface near the apex is gently drooped over the whole semi-span.

The mean surface arising from all these considerations and calculated by the programmes described above is illustrated in Fig. 11, in which cross-sections and chordwise sections have been combined to provide a three-dimensional view of the mean surface at its attachment incidence. The arbitrary function of y which enters the calculation of the mean surface has been chosen to make the trailing edge straight. The cross-sections show the characteristic droop of the leading edges required to produce attached flow at a positive lift coefficient, with the droop concentrated close to the leading edges towards the rear and spread over the whole cross-section at the front, as described above. These cross-sections are arranged lengthwise so that the centreline incidence is much larger at the front than the rear, giving the required shift of the centre of pressure forward from the aerodynamic centre. In the more familiar terminology developed for high-aspect-ratio wings, the mean surface can be described as having negative camber on the centreline, changing through inflected shapes to positive camber near the tip, with marked wash-out from root to tip.

The local load coefficient $l(x,y) = \Delta C_p$ corresponding to the attachment condition is shown in Fig. 12. The apparently arbitrary lengthwise stations at which this is drawn are those at which pressure measurements were to have been made on a wind-tunnel model. The decrease in level of $l(x,y)$ from front to rear is associated with the nose-up pitching moment. The negative values of $l(x,y)$ over the central part of the span towards the rear are a consequence of the attempt to keep the drag low by carrying load on the tips without carrying much total cross-load on the rear of the wing. In the cruising condition the incidence loading corresponding to $C_L = 0{\cdot}05$ would be superimposed on that shown in Fig. 12.

A volume distribution with a low wave drag intended to meet the main requirements of stowage, balance and structure on a transport aircraft of this planform was developed in parallel by J. Weber and

---

*If the lift and drag coefficients of the wing are C_L and C_D, and C_{D_0} is the zero-lift drag of the wing with the same volume distribution and top-and-bottom symmetry, we use the drag factor $K = \pi A(C_D - C_{D_0})/C_L^2$.

tested, both as a symmetrical wing and in combination with the mean surface just described, by A. O. Ormerod. Some preliminary results were quoted in Ref. 2 and are repeated here to indicate the measure of success achieved by the design method. At the design Mach number of 2·2, the attachment lift coefficient of 0·05 was produced at an incidence within one-tenth of a degree of the calculated attachment incidence. At $C_L = 0{\cdot}05$ the centre of pressure was 57·3 per cent of the length from the apex, i.e. less than 1 per cent of the length behind the intended position. At $C_L = 0{\cdot}1$, the intended cruising lift coefficient, the measured lift-dependent drag factor $K = \pi A(C_D - C_{D_0})/C_L^2$ was 1·93, which is marginally less than the value of 2·00 measured on the unwarped wing.* (Here C_{D_0} is the zero-lift drag of the unwarped wing.) These results indicate a substantial measure of success for the design procedure and calculation.

Although not relevant to the theme of the present report, the failure of the wing to trim at its design point should perhaps be mentioned. The low-speed aerodynamic centre of the unwarped wing was found to be some 1 per cent further forward than had been assumed and that of the warped wing was about 1 per cent further forward still. Consequently, with a centre of gravity providing neutral stability at the approach, the trimmed C_L at $M = 2{\cdot}2$ was only 0·08 instead of 0·10. There is every reason to think that, with the experimental results available, a completely successful re-design would be possible.

5.3. *The Design of a Lifting Surface in the Presence of a Short, Round Fore-Body*

For various reasons there is a case[2,34] for replacing the nose of the wing by a short, round fore-body, with the sharp-edged wing emerging from the body side some 30 per cent of the overall length back from the apex. Further aft the body will disappear into the wing thickness, so that the rear part of the configuration can be the same as that of the wings described earlier.

A simple way to reduce the interference of the fore-body on the lifting properties of the wing is to arrange the fore-body to point into the incident stream at the attachment incidence. There is then no body upwash field to interfere with the calculation of the warp distribution to produce the desired loading. For the warp distribution to be compatible with this body direction, the incidence of the wing must vanish at the apex. This is readily achieved by setting the coefficients $b_{n,1}$, $0 \leqslant n \leqslant N$, in equation (17) equal to zero. The body can then be carried forward from the gross wing apex into the wind direction and backward from it along the centreline of the gross wing. The lift carried on the body forward of the wing root will then be close to that postulated for the gross wing forward of the same station and, since this lift is small, the correspondence will be close enough for the properties of the configuration to be treated by the previous methods. Moreover, the upwash generated by the portion of the body between the gross wing apex and the leading edge root will also be close to that generated by the portion of the gross wing ahead of the root and will again be small.

A mean surface was designed for a gross wing along the same lines as indicated in the previous Section, with the additional restriction $b_{n,1} = 0$, and combined with a suitable thickness distribution derived by J. Weber. The plan-form is shown in Fig. 13.

The model resulting was tested by C. R. Taylor and preliminary results were quoted in Ref. 2. The attachment lift coefficient of 0·05 was again reached about one-tenth of a degree from the calculated attachment incidence. At $C_L = 0{\cdot}05$ the measured centre of pressure was rather over 1 per cent of the length of the gross wing behind its intended position. The required forward movement was slightly under-estimated so that the trimmed lift coefficient was again about 0·08. The measured lift-dependent drag factor, K, was 1·95 for the warped configuration, as against 2·05 for the symmetrical one, at $C_L = 0{\cdot}10$, $M = 2{\cdot}2$.

From this we may conclude that warp can be designed by the methods described as successfully for configurations with short fore-bodies as for wings alone, provided the bodies can be shaped to fit the flow field of the wing.

---

*There is already a favourable effect of thickness on lift-dependent drag in the case of the unwarped wing. On a very thin flat wing with sharp edges the resultant of the pressure forces on the wing is normal to the wing plane, so that the lift-dependent drag, $C_D - C_{D_0}$, is αC_L. The measured value of $\pi A \alpha C_L / C_L^2$ on the unwarped wing was 2·41 under the above conditions.

LIST OF SYMBOLS

a_n = Polynomial in x [equation (16)]

A = Aspect ratio

$b_{n,m}$ = Coefficient of a_n [equation (17)]

c = Length of wing

c_j = Coefficient of $s(x)$ [equation (18)]

C_L = Lift coefficient

C_p = Pressure coefficient

E' = Complete elliptic integral of complementary modulus

f, f_i = Tabular values [Fig. 4 and equation (33)]

h = Tabular interval [Fig. 4 and equation (33)]

K = { Cotangent of leading-edge sweep of delta wing; Lift-dependent drag factor

K' = Complete elliptic integral of complementary modulus

l = ΔC_p local load coefficient

$L(x)$ = Cross-loading

$L(x)$ = Lift acting forward of station x

M = Mach number

$P(x,\eta)$ = *See* equation (20)

$\bar{P}(x,\eta)$ = *See* equation (23)

q = $\frac{1}{2}\rho U^2$ kinetic pressure

$Q(x_1)$ = *See* equation (26) and Appendix A

$r(y)$ = Function inverse to $s(x)$

$s(x)$ = Local semi-span of wing

s_T = $s(1)$, overall semi-span of wing

U = Free stream speed

u,v = Characteristic coordinates in wing plane

x,y,z = Right-handed rectangular coordinates, origin at apex, Ox downstream, Oy to starboard

x_1, y_1 = Current values of x,y

α = Local incidence of mean surface of wing

β = $|M^2-1|^{\frac{1}{2}}$

δ,ε = *See* Fig. 4

Δ = Difference operator across wing plane

η = $y/s(x)$ or $y_1/s(x_1)$

λ = Streamwise surface slope of upper surface of volume distribution

ξ = *See* equation (30)

ρ = Density

ϕ = Disturbance velocity potential

REFERENCES

No.	*Author*	*Title, etc.*
1	D. Küchemann	Some considerations of aircraft shapes and their aerodynamics for flight at supersonic speeds. 2nd I.C.A.S. Conference, Zurich, 1960. *Advances in Aeronautical Sciences* 3, p.221 Pergamon Press, London, 1961.
2	A. Spence and J. H. B. Smith	Some aspects of the low-speed and supersonic aerodynamics of lifting slender wings. 3rd I.C.A.S., Stockholm, August, 1962. *Proceedings* p. 553. Spartan Books, Washington 1964.
3	D. Küchemann	Die aerodynamische Entwicklung von schlanken Flügeln für den Überschallflug. Jahrbuch 1962 der WGLR, pp.66–77; Brunswick 1962.
4	E. C. Maskell and J. Weber ..	On the aerodynamic design of slender wings. *J. R. Ae. Soc.* 63, p.709, 1959.
5	J. C. Cooke and M. G. Hall ..	*Progress in Aeronautical Sciences, 2,* Section 2 (ed.A.Ferri, D. Küchemann and L. H. G. Sterne) Pergamon Press, London 1962. Boundary layers in three-dimensions.
6	L. C. Squire	Further experimental investigations of the characteristics of cambered gothic wings at Mach numbers from 0·4 to 2·0. (A.R.C. R. & M.3310) December, 1961.
7	L. C. Squire	The characteristics of some slender cambered gothic wings at Mach numbers from 0·4 to 2·0. A.R.C. R. & M.3370, May, 1962.
8	C. R. Taylor	Measurements, at Mach numbers up to 2·8, of the longitudinal characteristics of one plane and three cambered slender 'ogee' wings. A.R.C. R. & M.3328, December, 1961.
9	P. Germain and R. Gibault ..	Quelques résultats sur les ailes delta portantes à traînée minimum en régime supersonique. *La Recherche Aéronautique* No. 61, pp.54–56, Nov.–Dec. 1957. *La Recherche Aéronautique* No. 63, p. 39, March–April 1958.
10	J. H. B. Smith	The problem of trim for a supersonic slender-wing aircraft. A.R.C. 21624, October 1959.
11	H. Lomax	Wave drag of arbitrary configurations in linearised flow as determined by areas and forces in oblique planes NACA RM A55A18, March 1955.
12	R. F. A. Keating	Low speed wind-tunnel tests on sharp-edged gothic wings of aspect ratio 3/4. A.R.C. C.P. 576, May 1960.

REFERENCES—*continued*

No.	*Author(s)*	*Title, etc.*
13	L. C. Squire	Measurement of lift and pitching moment on four ogee wings at supersonic speeds. A.R.C. C.P. 673, October 1962.
14	F. Walkden and J. H. B. Smith	Unpublished M.O.A. Report.
15	J. Weber	Design of warped slender wings with the attachment line along the leading edge. A.R.C. R. & M. 3406, September 1957.
16	G. M. Roper	Use of camber and twist to produce low-drag delta or swept-back wings, without leading edge singularities, at supersonic speeds. A.R.C. R. & M. 3196, December 1958.
17	M. Fenain	*Progress in Aeronautical Sciences* 1, Section 3 (ed.A.Ferri, D. Küchemann and L. H. G. Sterne). La théorie des écoulements à potentiel homogène et ses applications au calcul des ailes en régime supersonique. Pergamon Press, London 1961.
18	H. Portnoy	An extension of the method of generalised conical flows for lifting wings in supersonic flow. *Aero. Quart.* 14 (3), Aug. 1963.
19	M. A. Heaslet and H. Lomax	*General theory of high speed aerodynamics*, (ed. W. R. Sears), Section D, Supersonic and transonic small perturbation theory. O.U.P., London 1955.
20	G. J. Hancock	Notes on thin-wing theory at supersonic speeds. A.R.C. 20285, July 1958.
21	G. M. Roper	Formulae for calculating the camber surfaces of thin, swept-back wings of arbitrary planform with subsonic leading edges and specified load distribution. A.R.C. R. & M. 3217, June 1959.
22	J. C. Evvard	Use of source distributions for evaluating theoretical aerodynamics of thin finite wings at supersonic speeds. NACA Report No. 951, 1950.
23	J. H. B. Smith and K. W. Mangler	The use of conical camber to produce flow attachment at the leading edge of a delta wing and to minimize the lift-dependent drag at sonic and supersonic speeds. A.R.C. R. & M. 3289, September 1957.
24	P. Germain and M. Fenain ..	Détermination d'ailes en delta optimales à bord d'attaque sonique. *La Recherche Aéronautique* No. 86, Jan.–Feb. 1962.

No.	*Author(s)*	*Title, etc.*
25	P. Germain	Sur le minimum de traînée d'une aile de forme en plan donné. *C.R. Acad. Sci.*, Paris, 244, p.1135, 1957.
26	M. Fenain and D. Vallée ..	Application de la théorie des écoulements homogénes à la recherche de l'adaptation de certaines ailes en régime supersonique. O.N.E.R.A. Mémo Technique No. 14 (Part 2) 1959.
27	A. L. Courtney and A. O. Ormerod	Pressure-plotting and force tests at Mach numbers up to 2·8 on an uncambered slender wing of $p = \frac{1}{2}$, $s/c_0 = \frac{1}{4}$. A.R.C. R. & M. 3361,May 1961.
28	R. V. Clark	Aerodynamic design of wind-tunnel models of ogee planform. Handley Page Report Aero 343, November 1959.
29	E. Eminton	Pressure distribution at zero-lift for delta wings with rhombic cross-sections. A.R.C. C.P. No. 525, October 1959.
30	M. C. P. Firmin	The pressure distribution at zero-lift on some slender delta wings at supersonic speeds. A.R.C. C.P. 774, November 1963.
31	J. C. Cooke	Slender not-so-thin wing theory. A.R.C. C.P. No. 659, January 1962.
32	M. C. Adams and W. R. Sears	Slender body theory-review and extension. *J. Aeronaut. Sci.* 20, p.85, 1953.
33	L. C. Squire	Some applications of not-so-slender wing theory to wings with curved leading edges. A.R.C. R. & M. 3278, July 1960.
34	D. Küchemann and A. Spence	Unpublished M.O.A. Report.

APPENDIX A

Complete Expression for Local Incidence as Programmed.

With $P(x_1,\eta)$ as defined by equation (20), equation (22) becomes:

$$\pi\beta\,\alpha(x,y) = \int_1^{\bar{x}_1}\int_1^{1} \frac{P(x_1,\eta)-P(\bar{x}_1,-1)\sqrt{\frac{1-\eta}{1-\eta_1}\,\frac{\eta_2-\eta}{\eta_2-\eta_1}}-P(\bar{x}_2,1)\sqrt{\frac{1+\eta}{1+\eta_2}\,\frac{\eta-\eta_1}{\eta_2-\eta_1}}}{\{(1-\eta^2)\,(\eta-\eta_1)\,(\eta_2-\eta)\}^{\frac{1}{2}}}\,d\eta\,dx_1 +$$

$$+\int_{\bar{x}_1}^{\bar{x}_2}\int_{\eta_1}^{1} \frac{P(x_1,\eta)-P(\bar{x}_1,-1)\sqrt{\frac{1-\eta}{2}\,\frac{\eta_2-\eta}{\eta_2+1}}-P(\bar{x}_2,1)\sqrt{\frac{1+\eta}{1+\eta_2}\,\frac{\eta-\eta_1}{\eta_2-\eta_1}}}{\{(1-\eta^2)\,(\eta-\eta_1)\,(\eta_2-\eta)\}^{\frac{1}{2}}}\,d\eta\,dx_1 +$$

$$+\int_{\bar{x}_2}^{x}\int_{\eta_1}^{\eta_2} \frac{P(x_1,\eta)-P(\bar{x}_1,-1)\sqrt{\frac{1-\eta}{2}\,\frac{\eta_2-\eta}{\eta_2+1}}-P(\bar{x}_2,1)\sqrt{\frac{1+\eta}{2}\,\frac{\eta-\eta_1}{1-\eta_1}}}{\{(1-\eta^2)\,(\eta-\eta_1)\,(\eta_2-\eta)\}^{\frac{1}{2}}}\,d\eta\,dx_1 +$$

$$+P(\bar{x}_1,-1)\int_0^{\bar{x}_1}\frac{1}{\sqrt{(1-\eta_1)\,(\eta_2-\eta_1)}}\log\frac{(\sqrt{2}+\sqrt{1-\eta_1})^2\,\beta\,s(x_1)}{Q_1(x_1)}\,dx_1 -$$

$$-P(\bar{x}_1,-1)\int_0^{\bar{x}_1}\left\{\frac{1}{\sqrt{(1-\eta_1)\,(\eta_2-\eta_1)}}-\frac{1}{\sqrt{2(\eta_2(\bar{x}_1)+1)}}\right\}\log(\bar{x}_1-x_1)\,dx_1 -$$

$$-P(\bar{x}_1,-1)\frac{\bar{x}_1\,(\log\bar{x}_1-1)}{\sqrt{2(\eta_2(\bar{x}_1)+1)}}+$$

$$+P(\bar{x}_2,1)\int_0^{\bar{x}_1}\frac{1}{\sqrt{(1+\eta_2)\,(\eta_2-\eta_1)}}\log\frac{(\sqrt{2}+\sqrt{\eta_2+1})^2\,\beta\,s(x_1)}{Q_2(x_1)}\,dx_1 -$$

$$-P(\bar{x}_2,1)\int_0^{\bar{x}_1}\left\{\frac{1}{\sqrt{(1+\eta_2)\,(\eta_2-\eta_1)}}-\frac{1}{\sqrt{2(1-\eta_1(\bar{x}_2))}}\right\}\log(\bar{x}_2-x_1)\,dx_1 -$$

$$-P(\bar{x}_2,1)\frac{\bar{x}_2\,(\log\bar{x}_2-1)-(\bar{x}_2-\bar{x}_1)\,(\log(\bar{x}_2-\bar{x}_1)-1)}{\sqrt{2(1-\eta_1(\bar{x}_2))}}+$$

$$+P(\bar{x}_1,-1)\int_{\bar{x}_1}^{\bar{x}_2}\frac{1}{\sqrt{2(\eta_2+1)}}\log\frac{(\sqrt{2}+\sqrt{1-\eta_1})^2\,\beta\,s(x_1)}{Q_1(x_1)}\,dx_1 -$$

$$-P(\bar{x}_1,-1)\int_{\bar{x}_1}^{\bar{x}_2}\left\{\frac{1}{\sqrt{2(\eta_2+1)}}-\frac{1}{\sqrt{2(\eta_2(\bar{x}_1)+1)}}\right\}\log(x_1-\bar{x}_1)\,dx_1-$$

$$-P(\bar{x}_1,-1)\frac{(\bar{x}_2-\bar{x}_1)(\log(\bar{x}_2-\bar{x}_1)-1)}{\sqrt{2(\eta_2(\bar{x}_1)+1)}}+$$

$$+P(\bar{x}_2,1)\int_{\bar{x}_1}^{\bar{x}_2}\frac{1}{\sqrt{(1+\eta_2)(\eta_2-\eta_1)}}\log\frac{(\sqrt{1-\eta_1}+\sqrt{\eta_2-\eta_1})^2\,\beta\,s(x_1)}{Q_2(x_1)}\,dx_1-$$

$$-P(\bar{x}_2,1)\int_{\bar{x}_1}^{\bar{x}_2}\left\{\frac{1}{\sqrt{(1+\eta_2)(\eta_2-\eta_1)}}-\frac{1}{\sqrt{2(1-\eta_1(\bar{x}_2))}}\right\}\log(\bar{x}_2-x_1)\,dx_1-$$

$$-P(\bar{x}_2,1)\frac{(\bar{x}_2-\bar{x}_1)(\log(\bar{x}_2-\bar{x}_1)-1)}{\sqrt{2(1-\eta_1(\bar{x}_2))}}+$$

$$+P(\bar{x}_1,-1)\int_{\bar{x}_2}^{x}\frac{1}{\sqrt{2(\eta_2+1)}}\log\frac{(\sqrt{\eta_2+1}+\sqrt{\eta_2-\eta_1})^2\,\beta\,s(x_1)}{Q_1(x_1)}\,dx_1-$$

$$-P(\bar{x}_1,-1)\int_{\bar{x}_2}^{x}\left\{\frac{1}{\sqrt{2(\eta_2+1)}}-\frac{1}{\sqrt{2(\eta_2(\bar{x}_1)+1}}\right\}\log(x_1-\bar{x}_1)\,dx_1-$$

$$-P(\bar{x}_1,-1)\frac{(x-\bar{x}_1)(\log(x-\bar{x}_1)-1)-(\bar{x}_2-\bar{x}_1)(\log(\bar{x}_2-\bar{x}_1)-1)}{\sqrt{2(\eta_2(\bar{x}_1)+1)}}+$$

$$+P(\bar{x}_2,1)\int_{\bar{x}_2}^{x}\frac{1}{\sqrt{2(1-\eta_1)}}\log\frac{(\sqrt{1-\eta_1}+\sqrt{\eta_2-\eta_1})^2\,\beta\,s(x_1)}{Q_2(x_1)}\,dx_1-$$

$$-P(\bar{x}_2,1)\int_{\bar{x}_2}^{x}\left\{\frac{1}{\sqrt{2(1-\eta_1)}}-\frac{1}{\sqrt{2(1-\eta_1(\bar{x}_2))}}\right\}\log(x_1-\bar{x}_2)\,dx_1-$$

$$-P(\bar{x}_2,1)\frac{(x-\bar{x}_2)(\log(x-\bar{x}_2)-1)}{\sqrt{2(1-\eta_1(\bar{x}_2))}}. \tag{37}$$

In these expressions $Q_1(x_1)$ and $Q_2(x_1)$ are defined by:

$$\left.\begin{aligned}Q_1(x_1)&=\frac{\beta\,s(x_1)(1+\eta_1)}{x_1-\bar{x}_1}=\frac{\beta\,s(x_1)+x_1-x+\beta y}{x_1-\bar{x}_1}\\ Q_2(x_1)&=\frac{\beta\,s(x_1)(\eta_2-1)}{\bar{x}_2-x_1}=\frac{-\beta\,s(x_1)-x_1+x+\beta y}{\bar{x}_2-x_1}.\end{aligned}\right\} \tag{38}$$

To evaluate the three double integrals η is expressed in terms of ξ by:

$$\left.\begin{aligned} \eta &= \frac{1}{2}\xi(3-\xi^2) && 0 \leqslant x_1 \leqslant \bar{x}_1 \\ \eta &= \frac{1}{2}\left\{1+\eta_1+(1-\eta_1)\frac{1}{2}\xi(3-\xi^2)\right\} && \bar{x}_1 \leqslant x_1 \leqslant \bar{x}_2 \\ \eta &= \frac{1}{2}\left\{\eta_2+\eta_1+(\eta_2-\eta_1)\frac{1}{2}\xi(3-\xi^2)\right\} && \bar{x}_2 \leqslant x_1 \leqslant x\ . \end{aligned}\right\} \tag{39}$$

APPENDIX *B*

Programming the Calculation of the Derivatives of Complicated Expressions.

As explained in Section 3, it may well happen that the function expressing the ordinate, z, of the unwarped wing in terms of its location (x,y) on the planform is very complicated. In particular, z is likely to depend on a number of intermediate functions of x. Since $\partial^2 z/\partial x^2$ occurs in the integrand of equation (13), this presents a difficulty in the evaluation of the pressure distribution due to volume.

This difficulty is two-fold. First, both the derivation and the programming of the extended explicit formulation of $\partial^2 z/\partial x^2$ are liable to error and not easy to check. Second, the length of the programme needed to evaluate such a complicated expression may exceed the capacity of the high-speed store, thus requiring the transfer of fresh instructions from the backing store in the course of the calculation of $\partial^2 z/\partial x^2$. Since about 300 values of $\partial^2 z/\partial x^2$ are required to find the pressure at a point, this would increase the computation time significantly. As an example of what can be involved, this formula, taken from Ref. 28, may be instanced:

$$z(x,y) = \frac{s}{gf}\left\{\alpha(1-\eta^2)+\frac{1-\alpha}{(1+\beta^2\eta^2)^{\frac{1}{2}}}\,\frac{(1+\beta^2)^{\frac{1}{2}}-(1+\beta^2\eta^2)^{\frac{1}{2}}}{(1+\beta^2)^{\frac{1}{2}}-1}\right\} \tag{40}$$

where the intermediate functions are given by

$$f = \frac{2}{3}\alpha+\frac{1-\alpha}{(1+\beta^2)^{\frac{1}{2}}-1}\left\{\frac{(1+\beta^2)^{\frac{1}{2}}}{\beta}\log\left(\beta+(1+\beta^2)^{\frac{1}{2}}\right)-1\right\}$$

$$g = 0{\cdot}5x+x^2-0{\cdot}5x^5$$

$$s = 12x^2(1-x)$$

$$\alpha = 0{\cdot}75-0{\cdot}65x$$

$$\beta = 12{\cdot}5x(1+x^2)$$

$$\eta = 4y/g$$

and the notation is unrelated to that used elsewhere in this report.

The evaluation of the derivatives of such expressions is much simplified by programming the formulae for the derivatives of a quotient and a square root, for instance, as routines which can be used as often as desired, and by arranging for the function and its first two derivatives to be stored in consecutive locations. Suppose, as a simple example, that the function

$$\frac{(A(x))^{\frac{1}{2}}}{B(x)+(C(x)/D(x))^{\frac{1}{2}}} \tag{41}$$

and its first two derivatives are required. Then two sub-routines are first constructed. $R-1$, given values of $u(x)$, $u'(x)$, $u''(x)$ in locations i, $i+1$, $i+2$ and $v(x)$, $v'(x)$, $v''(x)$ in locations j, $j+1$, $j+2$, places u/v, $(u/v)'$, $(u/v)''$ in locations k, $k+1$, $k+2$, using the elementary formula for the derivative of a quotient. $R-2$, given values of $u(x)$, $u'(x)$, $u''(x)$ in locations i, $i+1$, $i+2$, places $u^{\frac{1}{2}}(x)$, $(u^{\frac{1}{2}}(x))'$, $(u^{\frac{1}{2}}(x))''$ in locations k, $k+1$, $k+2$. Then, assuming the values of

A, A', A''	are in locations	0, 1, 2
B, B', B''	„	3, 4, 5
C, C', C''	„	6, 7, 8
D, D', D''	„	9, 10, 11,

the procedure is as follows.

Set $i = 6, j = 9, k = 12$ and enter $R-1$, giving C/D, $(C/D)'$, $(C/D)''$ in locations 12, 13, 14.

Set $i = 12, k = 15$ and enter $R-2$, giving $(C/D)^{\frac{1}{2}}$, $[(C/D)^{\frac{1}{2}}]'$, $[(C/D)^{\frac{1}{2}}]''$ in locations 15, 16, 17.

Form the denominator of (41) and its first two derivatives in locations 18, 19, 20.

Set $i = 0, k = 21$ and enter $R-2$, giving $A^{\frac{1}{2}}$, $(A^{\frac{1}{2}})'$, $(A^{\frac{1}{2}})''$ in locations 21, 22, 23.

Set $i = 21, j = 18, k = 24$ and enter $R-1$, giving the required quantities in locations 24, 25, 26.

Although in such a simple example the gain in space in the computer is not significant, the programming is already much simplified and the algebraic manipulation is eliminated. In the example of equation (40) above, the use of these same two subroutines makes the computation practicable and saves much space in the computer.

TABLE 1

Values of $-\partial^2 z/\partial x^2$ *on Upper Surface of Wing of Section* 5.1

y \ x	0	0·1	0·2	0·3	0·4	0·5	0·6	0·7	0·8	0·9	1·0
0	0·225	0·810	0·540	0·150	0·000	0·060	0·225	0·225	0·075	0·135	0·000
0·016̇		1·605	0·885	0·315	0·015	0·030	0·345	0·270	0·120	0·015	0·000
0·033̇			0·375	0·420	0·105	0·195	0·150	0·285	0·270	0·120	0·000
0·050					−0·030	0·180	0·300	0·315	0·420	0·285	0·000
0·066̇						0·135	0·345	0·000	0·180	0·345	0·165
0·083̇							0·210	0·315	0·240	0·375	0·180
0·100							−0·135	0·360	0·315	0·405	0·270
0·116̇								0·165	0·390	0·375	0·225
0·133̇									0·675	0·375	0·300
0·150									0·450	0·465	0·300
0·166̇										0·600	0·330
0·183̇										1·065	0·360
0·200											0·405

TABLE 2

Values of $\partial z/\partial x$ *on Leading Edge of Upper Surface of Wing of Section* 5.1

x	0	0·1	0·2	0·3	0·4	0·5	0·6	0·7	0·8	0·9	1·0
$\partial z/\partial x$	0·250	0·200	0·096	0·060	0·052	0·050	0·050	0·050	0·050	0·050	0·050

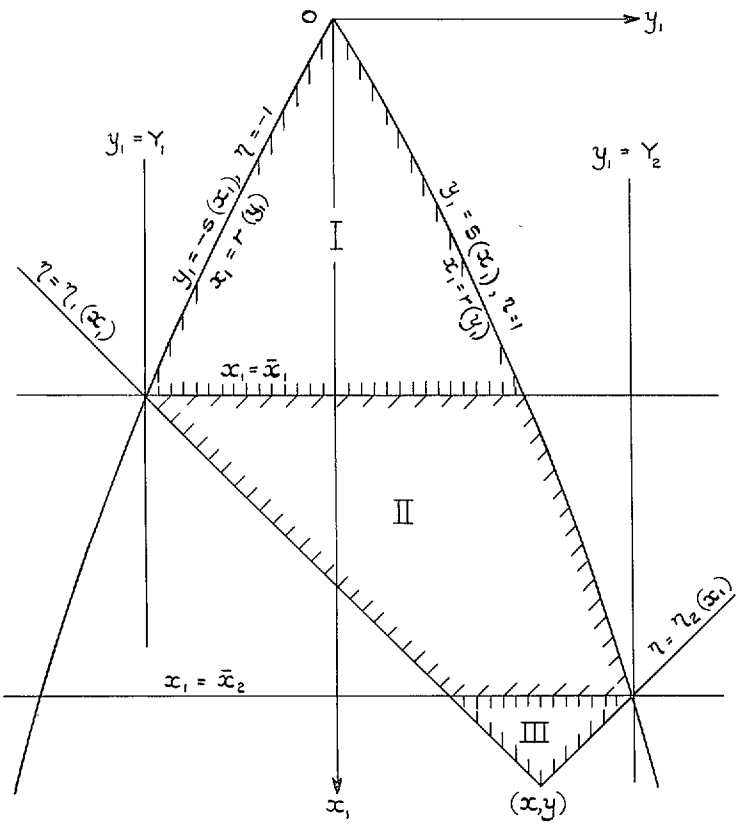

FIG. 1. Co-ordinates and regions of integration for calculation of warp.

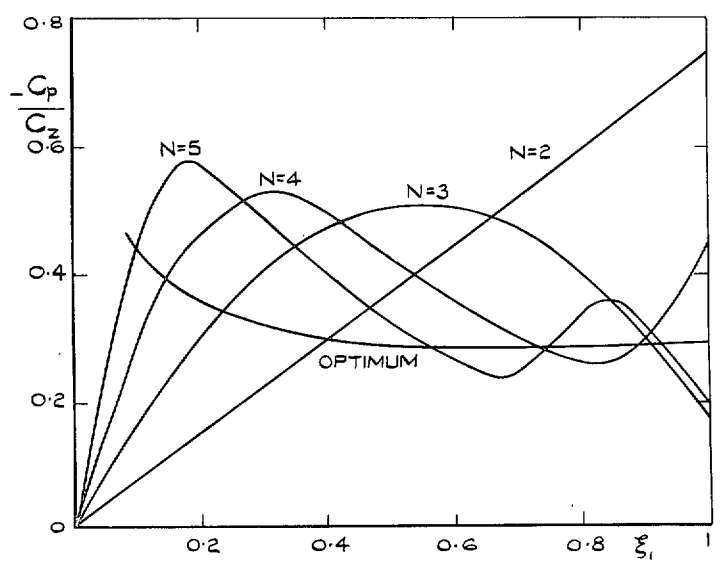

FIG. 2. Distribution of pressure along centreline of delta wings with sonic leading edges (after German and Fenain).

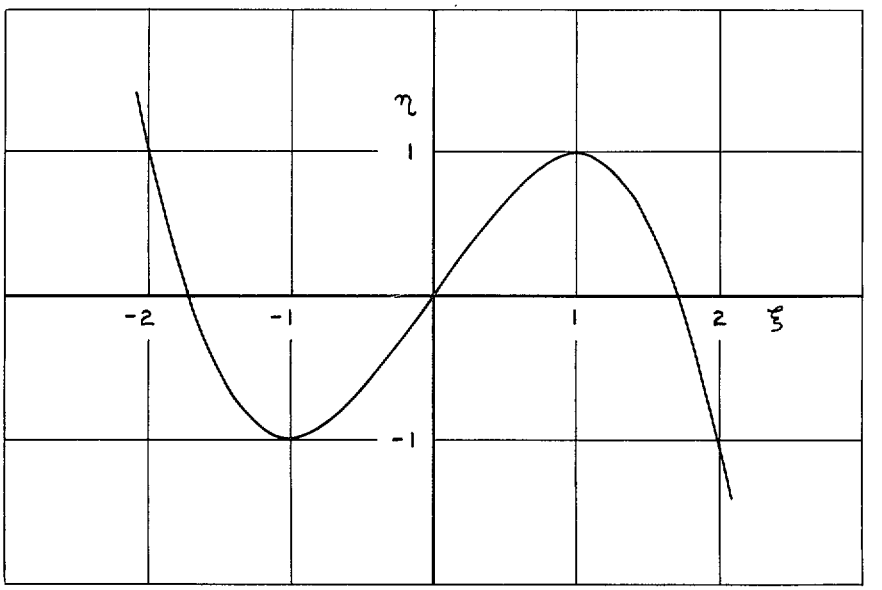

FIG. 3. Transformation of the variable.

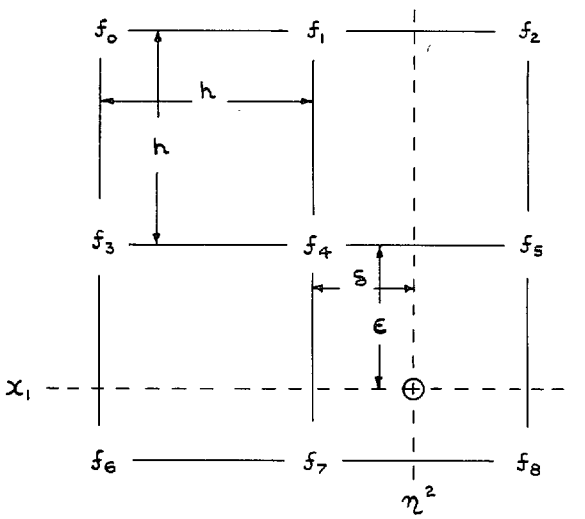

FIG. 4. Position of point in interpolation scheme.

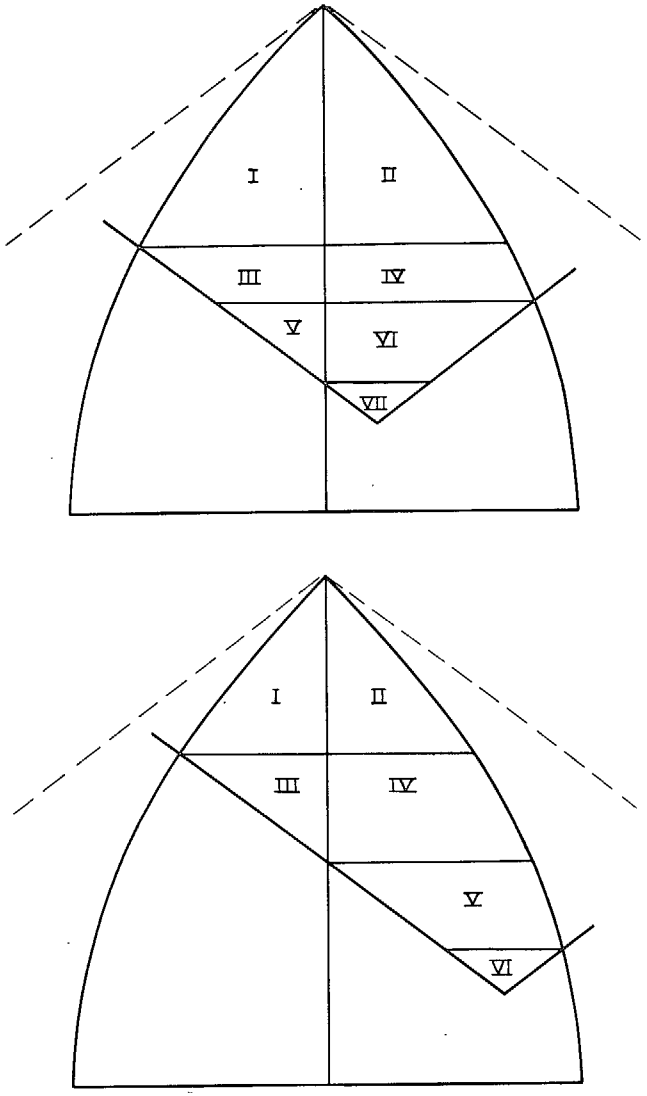

FIG. 5. Alternative arrangements of integration regions for calculating the pressure due to a distribution of volume.

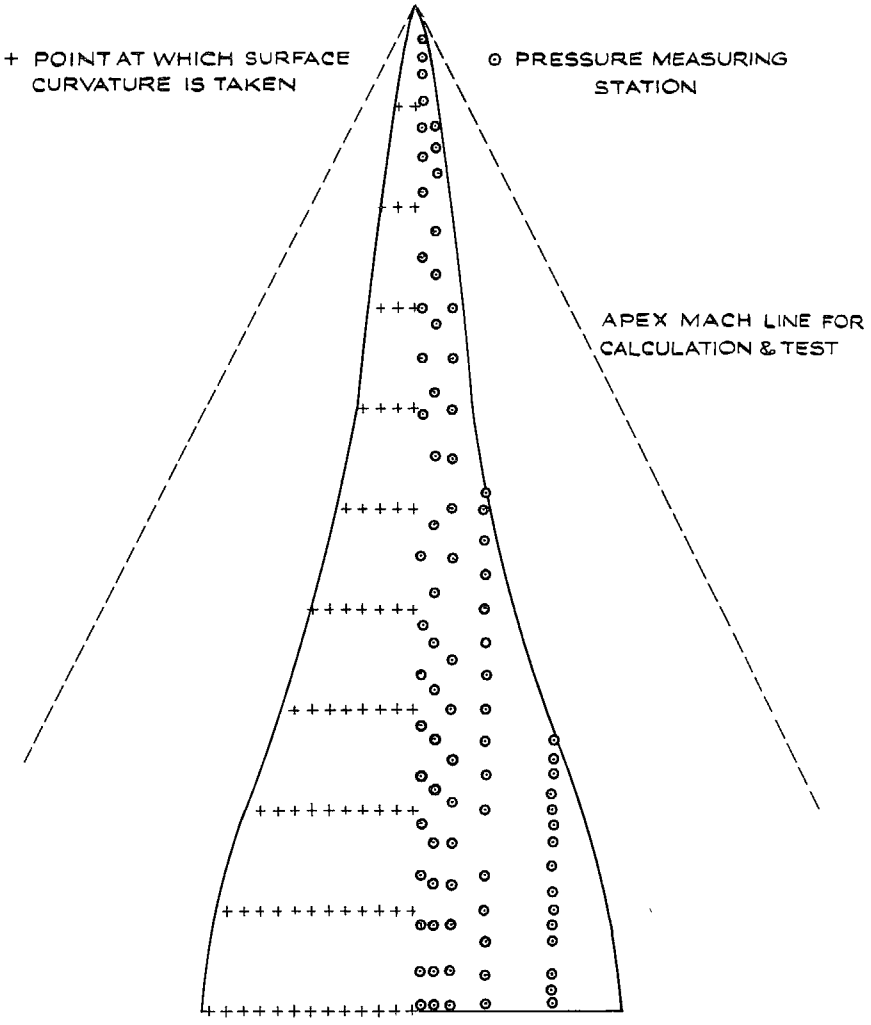

FIG. 6. Planform of wing of Section 5.1.

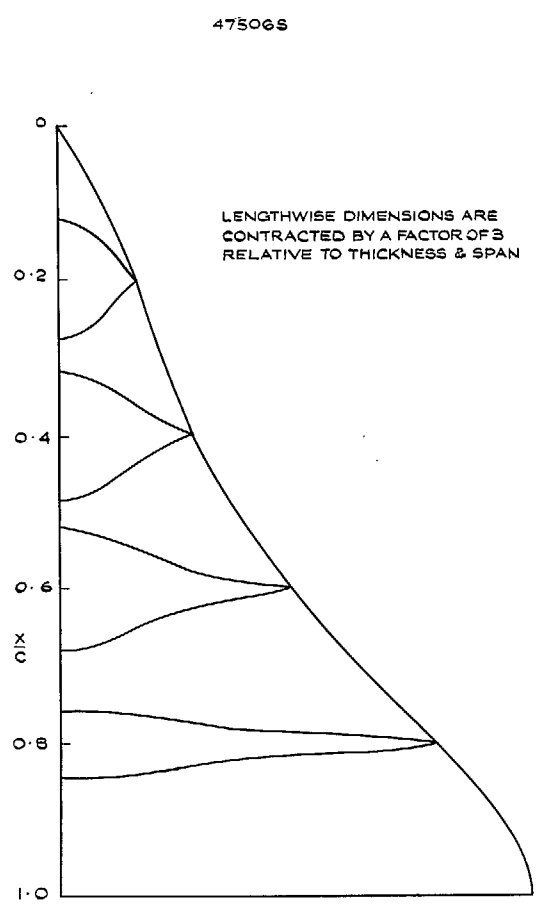

FIG. 7. Cross sections of wing of Section 5.1, (after Taylor).

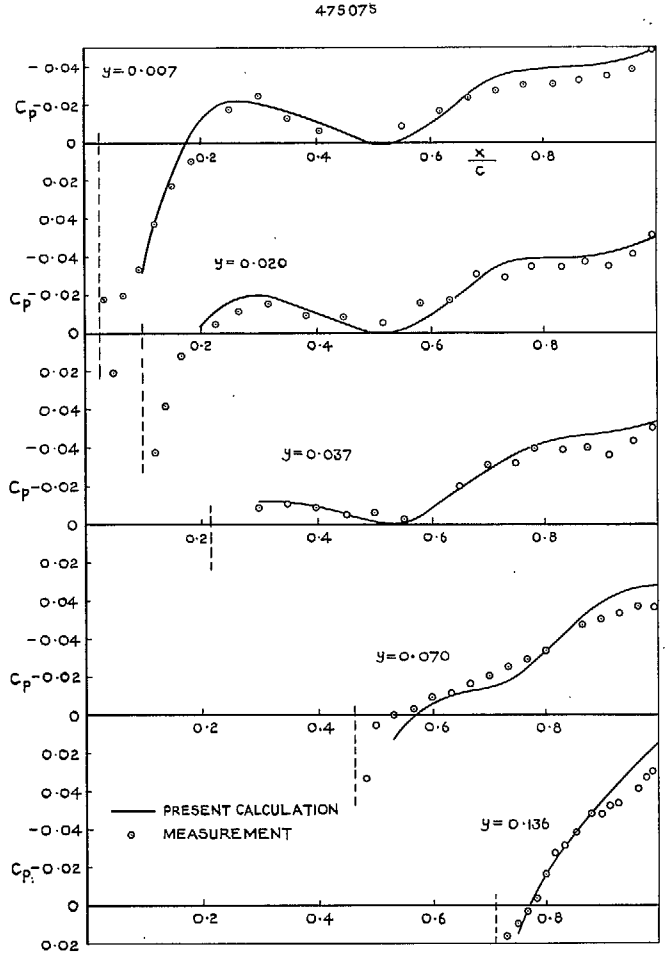

FIG. 8. Pressure Distribution: wing of Section 5.1, (after Taylor).

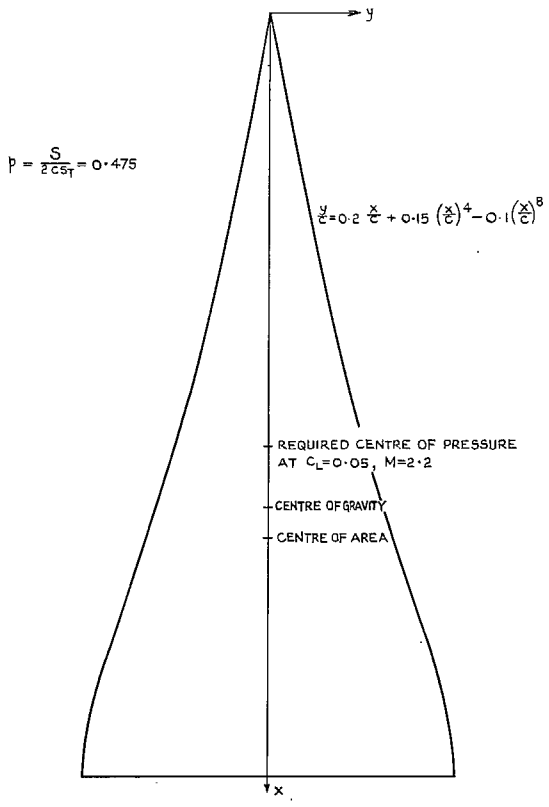

FIG. 9. Planform of wing of Section 5.2.

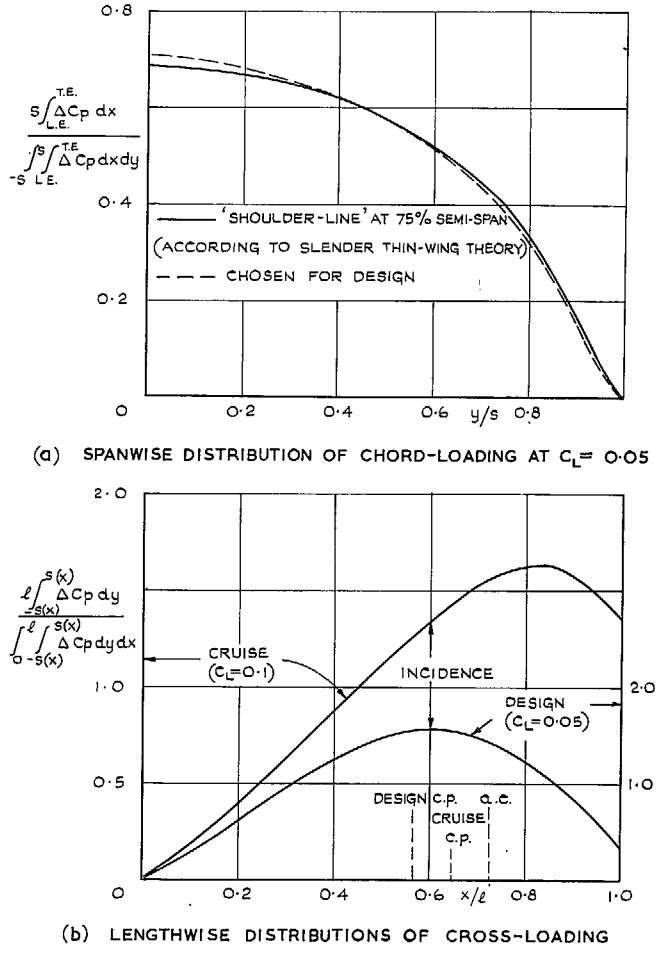

FIG. 10. Loading distributions for wing of Section 5.2 at $M = 2{\cdot}2$.

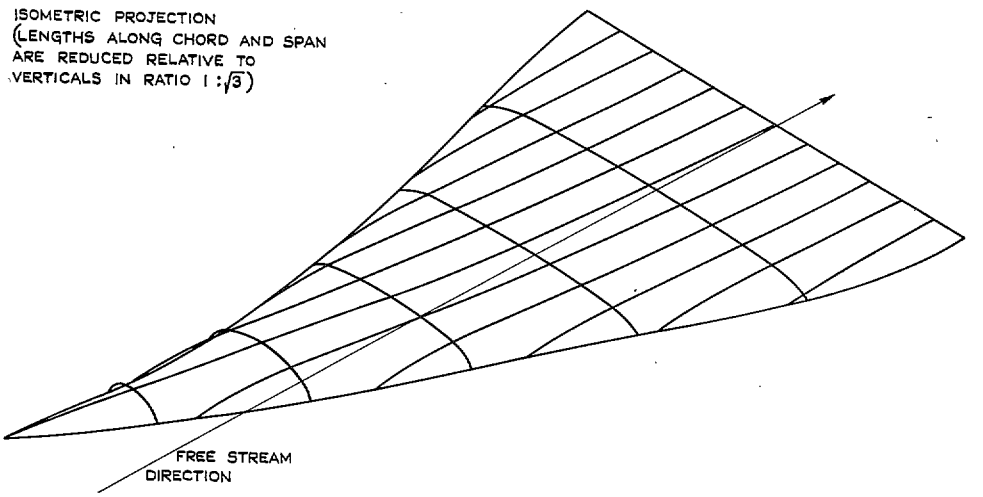

FIG. 11. Mean surface of wing of Section 5.2 at attachment incidence.

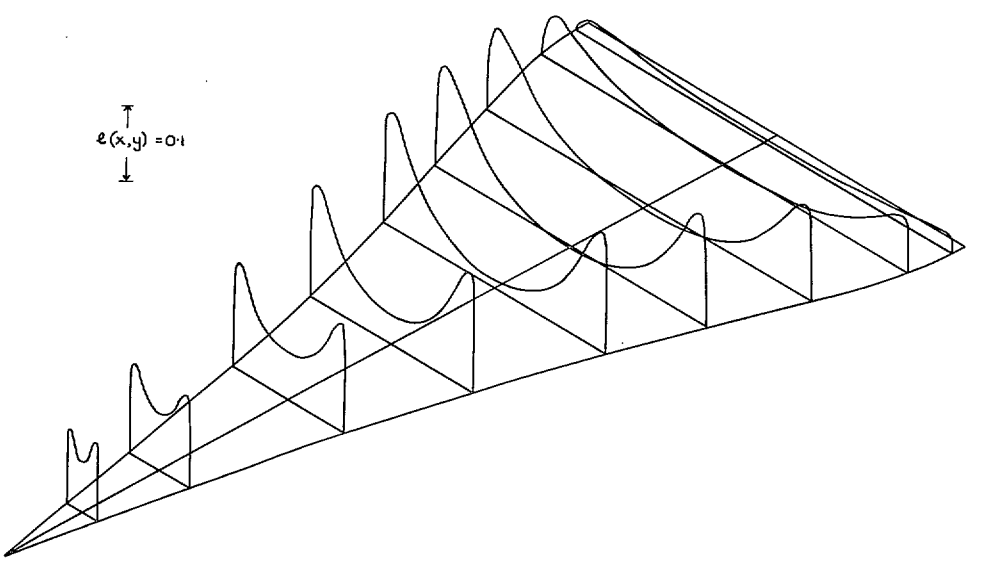

FIG. 12. Local load coefficient on wing of Section 5.2 at attachment incidence.

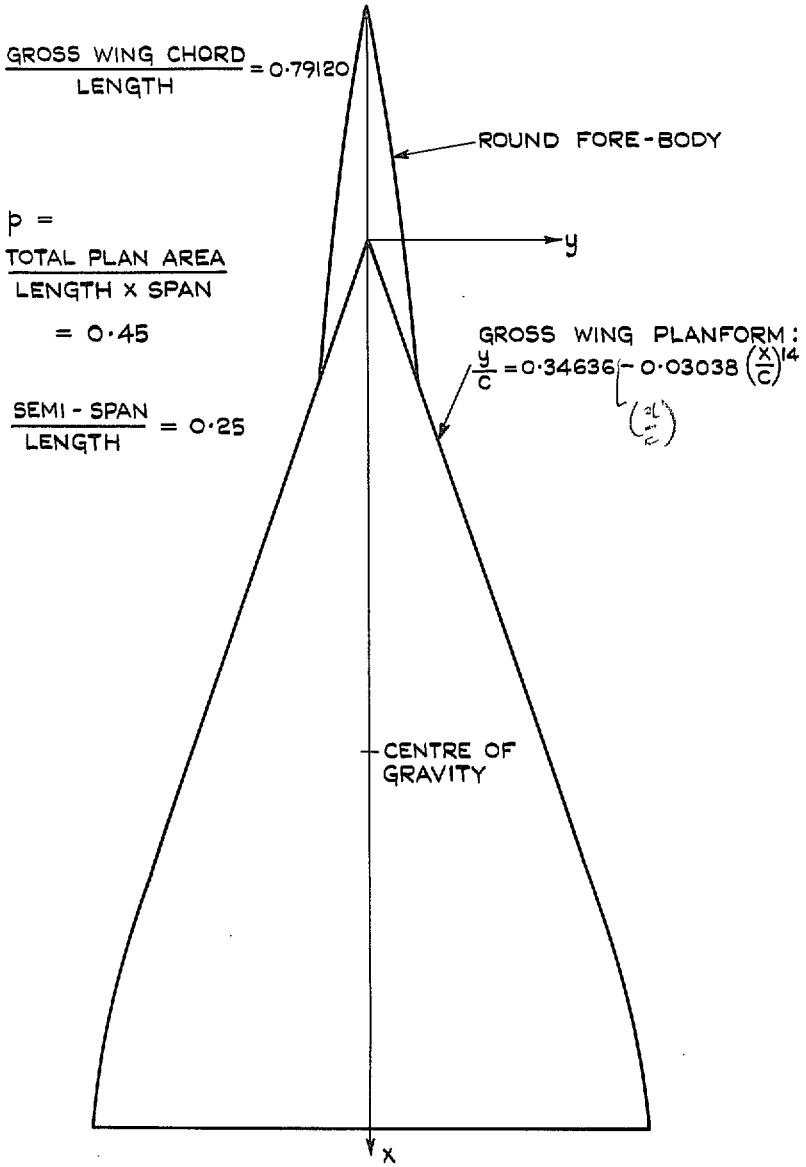

FIG. 13. Planform of wing-body combination of Section 5.3.

Printed in Wales for Her Majesty's Stationery Office by Allens (Wales) Limited.

Dd.125874 K5.

Published by
HER MAJESTY'S STATIONERY OFFICE

To be purchased from
49 High Holborn, London W.C.1
423 Oxford Street, London W.1
13A Castle Street, Edinburgh 2
109 St. Mary Street, Cardiff
Brazennose Street, Manchester 2
50 Fairfax Street, Bristol 1
35 Smallbrook, Ringway, Birmingham 5
7–11 Linenhall Street, Belfast 2
or through any bookseller

S.O. Code No. 23–3471